Continuous Gravity Observations at Mt. Somma-Vesuvius with a gPhoneX Gravimeter: In-Depth Instrumental Response Characterization and Tidal Model

U. Riccardi, S. Carlino, T. Pivetta, J. Hinderer, Séverine Rosat, G. Ricciardi

Continuous gravity observations at Mt. Somma-Vesuvius with a gPhoneX gravimeter: in-depth instrumental response characterization and tidal model

Riccardi U.[1,4]*, Carlino S.[2], Pivetta T.[2], Hinderer J.[3], Rosat S.[3], Ricciardi G.[2]

[1]Dipartimento di Scienze della Terra, dell'Ambiente e delle Risorse, Università di Napoli Federico II, Naples, Italy;
[2]Istituto Nazionale di Geofisica e Vulcanologia, Sezione di Napoli–Osservatorio Vesuviano, Naples, Italy;
[3]Institut Terre et Environnement de Strasbourg (UMR 7063), Université de Strasbourg/EOST, CNRS, Strasbourg, France.
[4]Research Group 'Geodesia', Universidad Complutense de Madrid, 28040 Madrid, Spain;
*Corresponding author

Abstract

We report on the results of about 9 months of gravimetric recordings acquired at Mt. Somma-Vesuvius volcano (Southern Italy) with the new generation relative gravimeter gPhoneX#116 (gPh#116), which is a gravimeter specifically designed for continuous gravity recording. We also present the outcomes of an intercomparison experiment of the gPhone#116 conducted at the J9 gravity observatory in Strasbourg (France). In this intercomparison, we were able to check the scale factor of the meter with a high degree of precision by means of an intercomparison with 2 superconducting gravimeters (SGs) and a FG5-type absolute ballistic gravimeter. Multiple calibration approaches allowed us to validate the manufacturer's original calibration constants to a level of 1% accuracy and 0.1% precision. Moreover, we carried out a comparative study of the noise level of the gPh#116 with respect to the SGs and other spring meters routinely used in both prospecting and time-lapse gravimetry. It turns out that gPh#116 exhibits lower levels at hourly time-scales than other compared spring gravimeters (Graviton, gPhone#054, Scintrex-CG5). It was also possible to carry out a detailed study of the instrumental drift, a crucial topic for reliable monitoring of the long-term gravity variations in active volcanic areas. In fact, a challenge in time-lapse gravimetry is the proper separation of the instrumental variations from real gravity changes eventually attributable to recharge or drainage processes of magma or fluids in the feeding systems of active volcanoes. A negative finding coming out from the intercomparison is that, even when applying the tilt correction, the gravimetric residuals obtained with the gPh#116 are an order of magnitude larger and quite inconsistent with those obtained with co-located superconducting gravimeters. We guess this problem could be overcome by installing the gravimeter on an auto-levelling platform.

From the analysis of the gravity records, a reliable tidal gravity model was derived, which we believe will help to improve the accuracy of volcano monitoring, as it will allow appropriate correction of tidal effects for both relative and absolute gravity measurements acquired in the area. Two further interesting elements arose from our study: 1) a peculiar cavity effect of the SV underground laboratory that seems to influence the tilt change; 2) the small residual gravity signals are time correlated with the rainfall peaks and are compatible with gravity decreases induced by increases in soil moisture above the gravimeter.

Keywords: Mt. Somma-Vesuvius, volcano monitoring, spring gravimeter, calibration, drift, continuous gravity records, tidal gravity model

1. Introduction

Over the past decades, the use of hybrid gravimetry, as defined by Okubo et al., (2002), i.e. based on the combined use of different gravity sensors (relative and absolute) and different data acquisition techniques (discrete on networks and continuous at permanent sites) has highlighted the enormous potential of using gravimetric monitoring to address a variety of geophysical tasks, ranging from hydrological problems to the monitoring of geothermal areas of economic interest and active volcanic areas. The high-precision repetition of gravity measurements collected on networks allows to reconstruct the time-variable field, while the continuous and precise monitoring of gravity allows both long-term and rapid changes to be detected. Coupling them in a hybrid approach can unleash significant potential for answering questions in many scientific fields, such as volcano monitoring, where mass redistributions occur on various temporal (from minutes to decades) and spatial (from a few to tens of kilometres) scales. A detailed review of terrestrial gravimetry applications including time-lapse monitoring can be found in Van Camp et al. (2017) and Crossley et al. (2013).
A number of papers have shown that time-lapse gravimetry can supply invaluable information about the source driving volcanic unrest (Gottsmann et al., 2006; Carbone et al., 2017; Battaglia et al., 2008; Williams-Jones et al., 2008). Indeed, gravity measurements are sensitive to changes in mass due to subsurface fluid flow, which is the breakthrough in understanding the source of the unrests or impending eruptions. Previous studies (e.g. Portier et al., 2018, Forster et al. 2021) have combined geothermal reservoir models with gravity data to look at the feasibility of using them for geothermal monitoring.

To obtain reliable gravimetric data, it is necessary to use instruments of adequate sensitivity, precision and temporal stability. Particularly in the monitoring of quiescent or closed-conduit volcanoes, the expected gravity signals related to mass redistribution processes at depth can be slow and of small amplitude (Rymer and Brown, 1989; Williams-Jones and Rymer, 2002). It therefore becomes crucial to adopt suitable acquisition and processing techniques and, in the case of using relative gravimeters, to obtain calibrations of a precision appropriate to the amplitude of the expected signals. Furthermore, for relative gravimeters, whether in discrete "survey" or continuous "recording" acquisition mode, it is of fundamental importance to feature the instrumental drift (Riccardi et al., 2011). In fact, we know that spring relative gravimeters are characterized by the so-called 'pink noise', related to the high energy in the low-frequency bands, due to the relaxation of the spring that generates an instrumental signal that can mask, if not even hide, the real gravity signals due to the slow processes of magmatic reservoir feeding at depth. In this sense, the availability of transportable superconducting gravimeters, thanks to their very low instrumental drift (a few μGal/year or tens of nm s^{-2}/year) (Hinderer et al., 2015), constitutes an important technological advancement in the service of geodetic volcano monitoring. However, at present, due to high costs, superconducting gravimeters are only available on a few active volcanoes (Carbone et al. 2017). A significant improvement in the performance of permanent gravimeters is the availability of spring gravimeters, specifically designed for recordings such as the gPhoneX (Micro-g LaCoste, Inc., 2013).

In the present research work we report on a new temporary realization of a recording gravity site at Somma Vesuvius (SV) volcano instrumented with a gravimeter specifically designed for continuous observations, the gPhoneX#116 (gPh#116). A significant part of this study is dedicated to the characterization of the instrumental response of the gPhoneX#116 (gPh#116) in terms of noise levels, calibration and study of the instrumental drift. The results of an intercomparison experiment between the gPh#116 and two superconducting gravimeters (iOSG#023 & iGrav#029) and an absolute ballistic gravimeter (FG5#206) conducted at the J9 gravimetric observatory in Strasbourg (France) are presented.

2. Mt Somma-Vesuvius and its recording gravity site

2.1. State of the art

The SV is a stratovolcano located east to the city of Naples, formed by an ancient small caldera (the Mt. Somma) and a youngest volcanic edifice (the Vesuvius) reaching a maximum altitude of 1,281 m asl (Fig. 1). It is structurally located along a main faults system trending NE-SW. The SV volcanic complex has been investigated by different geophysical and geochemical methods (Zollo et al., 1996; De Natale et al., 2001; Manzella et al., 2004; Cella et al., 2007; Caliro et al., 2011; Del Pezzo et al., 2013; D'Auria et al., 2014; Linde et al., 2017) providing important insight in understanding its structure and dynamic. Due to its peculiar location, within densely urbanised areas, where some seven hundred thousand people live, including large sections of the city of Naples (Italy), Vesuvius is one of the most dangerous volcanoes on Earth. Its past eruptions have ravaged cities and claimed thousands of lives, the well-known eruption of 79 A.D. being just one example; the last volcanic activity took place in March 1944. Therefore, although SV is currently in a quiescent state, it is one of the best monitored volcanoes in the world. The obvious main objective of this monitoring is to recognise possible precursors of imminent or future eruptions. Time-lapse gravimetry is one of the geophysical disciplines that form part of the complex multi-parameter geophysical and geochemical monitoring programme of SV. In particular, gravimetry is used in an integrated way with other geodetic techniques such as GNSS, InSAR, tide gauges and tiltmetry (Fig. 1).

The present quiescence of the volcano shows a dynamic characterized by a quite persistent (hundreds of events per years) and low energy seismic activity (maximum duration magnitude M_d= 3.6) (www.ov.ingv.it) which is mainly located between the volcanic edifice and a depth of 4 km b.s.l.. A minor cluster of earthquakes occurrence is located between 5 km and 8 km b.s.l (D'Auria et al., 2014). The base of the latter level roughly corresponds to a rheological transition possibly throughout a zone of partial melting of rocks (Zollo et al., 1996; Carlino 2018). The stress generating the shallower seismicity was correlated to the loading due to the weight of the volcano edifice, which responds with a slow deformation and spreading due to different rheology of the deeper clays strata (Borgia et al., 2005). The deeper seismicity is possibly the result of the interaction between the regional stress field and the dynamic of the hydrothermal system of the volcano (Chiodini et al., 2001; D'Auria et al., 2014). Geodetic data collected for monitoring purposes on **Ne**apolitan **Vo**lcanoes **C**ontinuous **GPS** (NeVoCGPS) network as well as DInSAR data from the last few decades at SV show that the central part of the volcano is undergoing a slight subsidence with a maximum rate of about 1-2 cm/yr along the crater axis (De Martino et al., 2021). In particular, the data provided by the NeVoCGPS network operated by the INGV (Osservatorio Vesuviano) highlight a clear difference in the subsidence rate between the stations located at the base of the Vesuvius crater and within the caldera structure and those located outside the caldera structure (De Martino et al., 2021). At the present, a slight fumarole activity with temperature around 60°C occurs just inside the crater of Vesuvius. The fumarolic fluids have a typical hydrothermal signature with major content of H_2O and a rich CO_2 gas phase. The high-temperature hydrothermal system (~ 450°C) feeding the fumarole activity is located along the volcano conduit at a depth of about 2km (Chiodini et al., 2001).

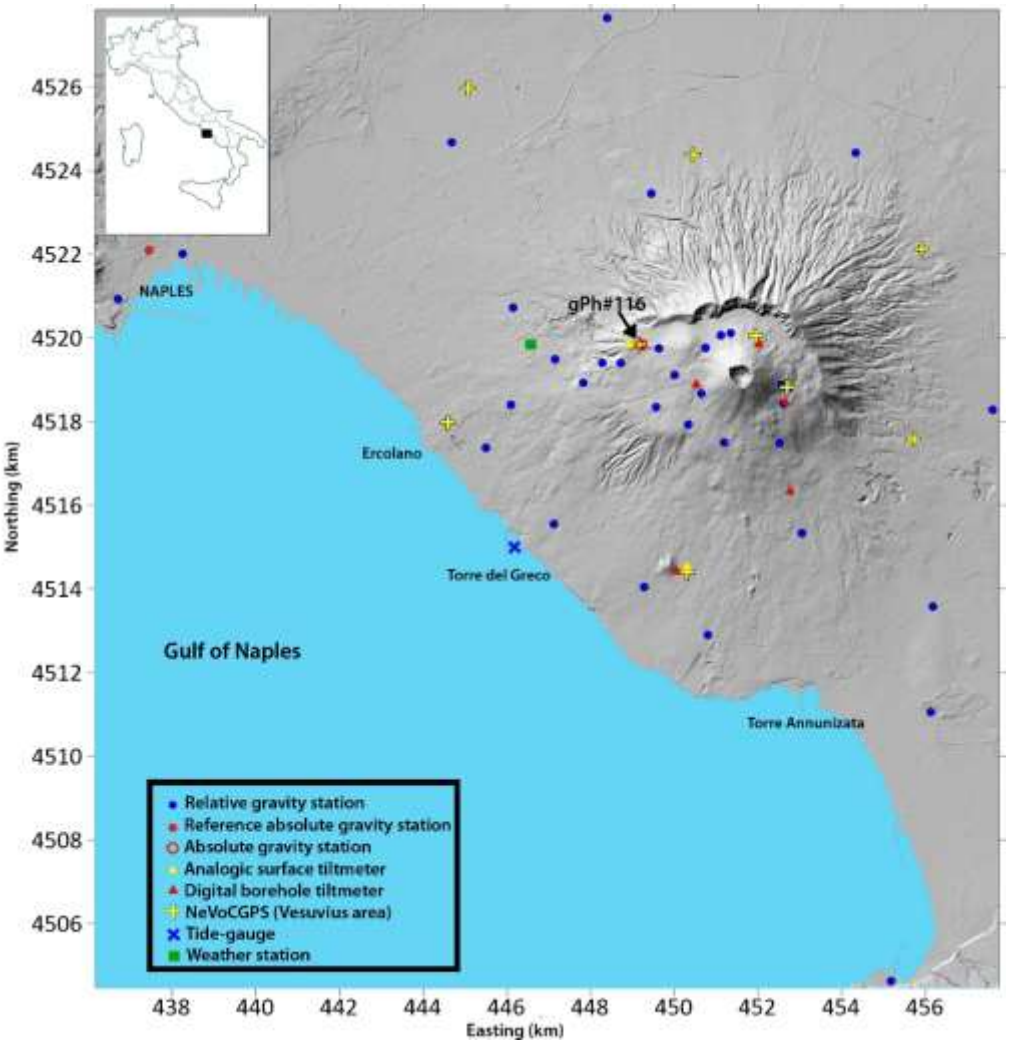

Fig. 1 *Mt. Somma-Vesuvius geodetic monitoring networks (www.ov.ingv.it) with indication of the position of the permanent gravity station (gPh#116).*

A several decades-long experience with hybrid time-lapse gravimetry for volcanic monitoring is available at SV. In fact, time-variable gravimetry survey have been performed there since 1982, even if at a limited number of stations; only since 2003 a most stable gravity monitoring network was established. Since 2003 the INGV (Osservatorio Vesuviano) is performing yearly time-lapse gravity measurements on a network of more than 30 gravity stations in the Vesuvius area using the relative D model LaCoste & Romberg gravimeter (LCR-D85) (Berrino et al., 2013). All the surveys are referred to an absolute reference station located outside the volcanic area, in the city centre of Naples (Largo San Marcellino), which is considered a stable site. The configuration of the gravity network at Vesuvius has changed throughout the years, in particular the number of the stations has increased and now it includes 36 stations. Analyses of both long-term and short-term gravity variations were performed by Berrino et al., (1999) and Berrino et al., (2013), showing that only in the former case significative changes occurred. As the authors consider negligible the ground deformation, they conclude that from 1982 to 2012 a considerable redistribution of mass occurred at SV, essentially by density change at constant volume possibly due to fluids migration in unsaturated porous medium (Berrino et al., 2013).

Even for continuous gravity recordings there is a very long tradition on SV. In fact, first attempts to collect continuous gravity observations date back to the1960s (Imbò et al., 1965); see Riccardi et al. (2008) and Berrino et al. (2006) for a detailed history of gravity records on SV.

In the same station, where the gPh#116 has been installed, the LCR, model D N°126 (LCR-D126) has operated since the late 1980s till early 2000s. It was equipped with a homemade feedback system implemented at the Royal Observatory of Belgium in Brussels (van Ruymbeke, 1991). This feedback has always suffered from a strong dependence on thermal variations, albeit they are very small in the laboratory, leading to strong and highly non-linear instrumental drifts. In addition, the data acquisition system has always had synchronisation issues and was severely limited by the clock drift. Although the LCR-D126 gravimeter was calibrated in the 1990s with the superconducting gravimeter SG-TT70-T015 operating at that time at Brasimone lake (Bologna-Italy), and calibrated on the same occasion with the absolute gravimeter FG5#206 of the French Strasbourg group (Riccardi et al., 2002; Baldi et al., 1999), the tidal analyses have always led to results that are difficult to reconcile with the expected theoretical values (Berrino et al., 2006; Riccardi et al., 2008). Besides, the proved bad sealing of the core spring sensor, which usually degrades over time, has always led to incoherent response of the gravimeter to the ambient pressure fluctuations leading to poor quality of some important diurnal (K1, mainly when not separated from P1 and S1 for record lengths < 200 days) and semi-diurnal (S2, K2) waves. Moreover, the bad synchronization made problematic the reliable determination of the tidal phase lags and the consequent adjustment of the ocean tide loading effects.

2.2 The New Temporary Recording Gravity Station at Mt. Somma-Vesuvius

A new recording gravity station has been temporary established on SV, located at the historical building of the Vesuvius Observatory (fig. 1). The station belongs to the monitoring relative gravity network, spanning the Vesuvian area, periodically surveyed since 1982. The permanent station is set on a concrete pillar located in a room of an artificial cave, 20 m deep, hosting other geophysical instruments (Berrino *et al*., 1997); the room has a very good thermal stability (daily about 0.1°C, annual within 2°C temperature excursion

The installation site is very close (< 50m) to an absolute gravity station established on the volcano in 1986 (Berrino, 2000), in the historical building of the Vesuvius Observatory, where the last measurement was collected in 2010 (Berrino et al., 2013).

The need to install a new gravity recording station at SV stems from the fact that although gravimetric recordings had already been acquired in the 1960s and on a regular basis since the late 1980s, as aforementioned, the previous stations had always been instrumented with gravimeters that were not specifically suitable for recording (Riccardi et al., 2008).Furthermore, as the Vesuvius underground laboratory is a relatively low-noise site, the performance of the new gPhoneX116 (gPh#116) purchased by the INGV needed to be tested before being installed in the Campi Flegrei area, that presently is undergoing an unrest.

In the 70s LCR company initiated the production of special land gravimeters, called ET (Earth Tides), equipped with a controlled double oven to ensure a very stable internal temperature, ad-hoc designed to meet the requirements of high precision recording of gravity tides. Since then the different designs have evolved through better performing permanent recording gravimeters like the Graviton Electronic gravimeter (Graviton EG) released in the 90s, but improvements in electronics have not always met expectations. More than 10 years ago, Microg-Lacoste Inc. started the production of a new generation of portable Earth tide gravimeter, named gPhone and more recently gPhoneX. The gPhone is essentially a double oven LCR, model G meter, but smaller in size than the former ET. The feedback system is the Aliod beam nulling system providing precise digital measurements at the level of 1 nm s^{-2} (0.1 μGal) (Microg-LaCoste, 2013). Furthermore, due to the high sealing efficiency of the core sensor, the gPhone has shown to be almost insensitive to humidity and buoyancy effects, which

allows for a consistent meter response to atmospheric pressure fluctuations (Riccardi et al., 2011). The synchronization accuracy of the data logger is done through a pps (pulse-per-second) clock device and a GPS clock antenna; this is pivotal for precise tidal observations.

3. Data Analysis and Results

The following sections present the data sets used in this study and report on the analyses conducted on the gravity records acquired at the J9 gravity observatory located near Strasbourg (France) and on the SV with the gPh#116.

The first two sections present an intercomparison experiment conducted at the J9 gravity observatory located near Strasbourg (France), where gravity records have been acquired for over 60 years, and for the last 40 years with the aid of superconducting gravimeters (Calvo et al., 2016). This experiment was planned to achieve a very accurate determination of the instrumental response of the gPh#116 and its performance. In particular, the scale factor provided by the manufacturer was verified through relative and absolute calibration by intercomparison with superconducting gravimeters and an absolute ballistic gravimeter. In addition, noise levels were analysed and an in-depth study of the time evolution of instrumental drift was conducted.In the last section, the analyses of the gravity recordings collected at Mt. Somma-Vesuvius are described.

3.1 J9 Experiment: Relative calibration of the gPh#116 by Superconducting gravimeters & Drift assessment

During the intercomparison the meter was located on a pillar in the same room as the iOSG#023, about 3 meters away from it (Fig. 2) and nearly 70 days of continuous gravity record were collected (Fig. 3). For the calibration experiment data from the SG iGrav#029 were also available (Fig. 4). 1 Hz data are collected, then the routine pre-processing steps are applied to the gravity records consisting of: a) decimation from 1 s to 60 s sampling rate; same decimation filter is applied to the gravity records collected with the three gravimeters (gPh#116, iOSG#023 and iGrav#029); 2) cleaning of the spikes, essentially due to far and near-field earthquakes; 3) modelling of the drift.

The drift of the two SGs is modelled by a least squares fitting with a first-degree polynomial (Fig. 4). This is a reasonable assumption considering that several authors (e.g. Hinderer et al., 2022) have shown that the exponential drift term in SGs vanishes a few months after installation. The iOSG#023 and iGrav#029 have been operating at J9 since 2016 and 2017, respectively (Hinderer et al., 2022). Furthermore, in the short time window used for the intercomparison (about 70 days), the higher-order polynomial terms in the drift can be considered negligible in any case.

As required for a mechanical spring gravimeter, special care was taken in estimating the drift of the gPh#116. It is recognised that compared to SGs, spring gravimeters, including the special ones designed for gravity records, such as the gPhoneX, have a much larger instrumental drift (up to thousands of $nm \cdot s^{-2}$ per year, Fig. 3b) due to the properties of the spring itself (metal or quartz) and its suspension. The instrumental drift usually dominates records collected with spring meters strongly limiting their use for studies aimed at detecting long term gravity changes. In fact, in some geodynamical context, where the mass budget assessment is needed, e.g. for active volcanoes processes of magma chamber refilling, or hydrology as well as geothermal reservoir monitoring, where the study of groundwater depletion or recharge is targeted, it is pivotal to discriminate between instrumental and real gravity changes. The first part of the record (about 15 days), from 6 to 22

October 2022, displays most of the gPhoneX initial relaxation after its installation. This is a typical behavior of the gPhone showing a more or less long non-linear relaxation, starting soon after initial installation, turning off, shortage of the electrical power or even shutdowns due to storms or whatever power accidents followed by a quasi-linear drift (Riccardi et al., 2011; Fores et al., 2019). It is quite evident (Fig. 3) that the main contribution of the higher degree polynomial (3rd degree) is to correct the end of the initial relaxation that persisted few days after the first 15 discarded days. Fores et al. (2019) have shown that a significant contribution to the drift may come from the tilt change over time. Indeed, unlike the SGs, which are equipped with an active compensation system of the tilt changes, based on thermal levelers (Goodkind, 1999; Riccardi et al., 2009), spring recording gravimeters are affected by tilt changes. In recent years, several companies have produced self-levelling platforms or individual research groups have developed some homemade ones (Fores et al., 2019); in our case this was not currently available. In the case of the instruments designed for recordings, usually it is possible to acquire the signal of two inclinometers oriented at 90° (Cross & Long Level) that provide data useful for post-processing corrections of tilt changes. Tilt variation translates into an apparent gravity change, and this is why this has to be considered as a contributing source to the instrumental drift. Actually the measured gravity has reached to its maximum when the sensitive axis of the gravity meter is aligned with the local gravity. When tilted, the gravity value measured by the sensor is reduced by the cosine of the angle between the sensitive axis of the sensor and the true vertical axis defined by local gravity. Assuming the gravimeter is initially set correctly to zero or negligible tilt angle, the measured gravity is given by

$$g_{measured} = g_0 cos\varphi \qquad (1)$$

where the angle φ is the measured angle between the local gravity and the vertical axis of the instrument. The value g_0 is the local maximum gravity when there is no tilt. For small angles, the cosine of the angular deviation can be approximated as a product of the cosines of the two orthogonal horizontal tiltmeter angles (x & y or Cross & Long. levels)

$$cos\varphi = cos\theta_x cos\theta_y \qquad (2)$$

The influence of gravimeter tilt on gravity measurement can be formulated as (Scintrex, 2008):

$$g_{(\vartheta_x,\vartheta_y)} = g_0 - g(1 - cos\varphi) \qquad (3)$$

The correction (Δg_{Tilt}), which is always positive, since the off-level axis measures the reduced gravity, is given by:

$$\Delta g_{Tilt} = g_0 - g_{(\vartheta_x,\vartheta_y)} = g(1 - cos\varphi) \qquad (4)$$

The difference between the gravity g and the projection $gcos\varphi$ of g onto the gravimeter axis is $\frac{g}{2}\varphi^2$, to the second order in φ. Of course, the apparent gravity $gcos\varphi$, which is measured by the gravimeter, is smaller than g. Assuming g = 9.8×10^9 nm s^{-2}, the apparent decrease in gravity (or tilt admittance) is about -4.9×10^{-3} nm/s^2/μrad^2 (Riccardi et al., 2009).

Figure 5a displays the time variable tilt experienced by the gPh#116 at J9 observatory. Between its installation on 6 October 2022 and 14 December of the same year, the inclination of the gPhoneX#116 was not controlled, but no manual levelling was required (Fig. 5a). The tilt varied by a few tens of analogue-to-digital converter (AD) units per week (1 AD is approximately 0.6 μrad; based on the scaling factors provided by the manufacturer), although the temperature at J9 was extremely stable. Level outputs are converted from AD units to tilt units (μrad) with the scale factors provided by the manufacturing company (Scintrex-Micro-g LaCoste), then multiplied by the tilt admittance factor to

obtain the apparent gravity change due to the tilt (Fig. 5b). The tilt correction enables us to separate the different sources contributing to the drift. As aforementioned, this is a quite critical task to be accomplished when the long-term gravity changes are the main goal of the gravity observation, as it is the case for active volcano monitoring. In that case the main target is the proper detection of eruptive precursors, namely the underground magma and/or fluid dynamics (feeding or drainage of plumbing systems).

All gravimeters used in this experiment are equipped with a barometer to monitor changes in atmospheric air pressure (Fig. 4c), which is routinely taken into account in the high-precision analysis of gravity recordings; the pre-processing steps 1) and 2) mentioned above were also applied to the air pressure records. After passing through the pre-processing steps, the 60 s gravity and air pressure records collected with the gPh#116 and the two SGs (Figs. 3 & 4) were analyzed with ET34-X-V80 software system for tidal analyses (Schüller, 2020). The tidal analysis was performed to obtain a significant number of tidal wave groups consistent with the length of the recordings, in accordance with the Rayleigh's criterion (Ducarme & Schüller, 2018). The results of tidal analyses (Table S1) in terms of tidal parameters, namely delta or gravimetric factors (δ_n) and phase lags (φ_n), where n stands for the degree of the harmonic development of the tide-generating potential, are used to calibrate the gPh#116 with respect to the SGs; a more detailed description of the physical meaning of the tidal parameters as well as of the different software for tidal analyses can be found in Riccardi et al. (2023).

Under the assumption that the SGs are accurately calibrated both in amplitude and phase (Hinderer et al., 2022), the procedure, consisting in comparing the tidal analyses through the delta ratios and phase difference ($\Delta\varphi = \varphi_{gPh\#116} - \varphi_{Ref.Inst.}$), allows a precise calibration both in amplitude and phase of the gPh#116 (Tab. 1).

Table 1 *Results of the relative calibration of the gPhone#116 retrieved from the tidal analyses performed on the 3 gravimeters for the better resolved waves; δ-Ratios are Ref.Instrument/gPh#116; bold indicates larger amplitude waves; WMean stands for weighted mean according to the tidal wave amplitude*

Wave	**iOSG#023**		**iGrav#029**	
	δ-Ratio	Error	*δ-Ratio*	Error
O1	1.0004357	0.000168	1.000209	0.000168
K1	**0.9994986**	**0.000116**	**0.999226**	**0.000116**
N2	1.0015732	0.001211	1.001284	0.00121
M2	**1.0001939**	**0.000111**	**0.999958**	**0.000111**
WMean	1.000075517	0.000190079	0.999825237	0.00019003

The phase lag between gPh#116, iOSG#023 and iGrav#029 leading negative, for the largest amplitude and better resolved tidal wave (M2), is 2.9 ± 0.8 s and 0.9 ± 0.8 s respectively, meaning that there is an unsignificant phase lag of gPh#116 with respect to the iGrav#029.

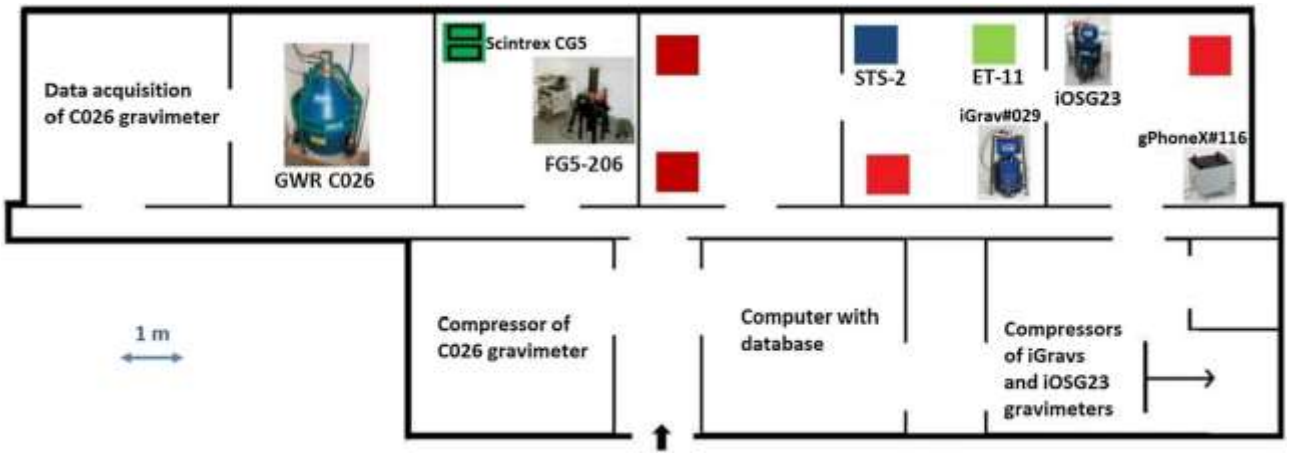

Fig. 2 *Floor plan of the Strasbourg Gravimetric Observatory (J9) indicating the location of the gPhoneX#116 and the other gravimeters used for this study (iGrav#029, iOSG#023 and FG5-206) (modified from Hinderer et al., 2022).*

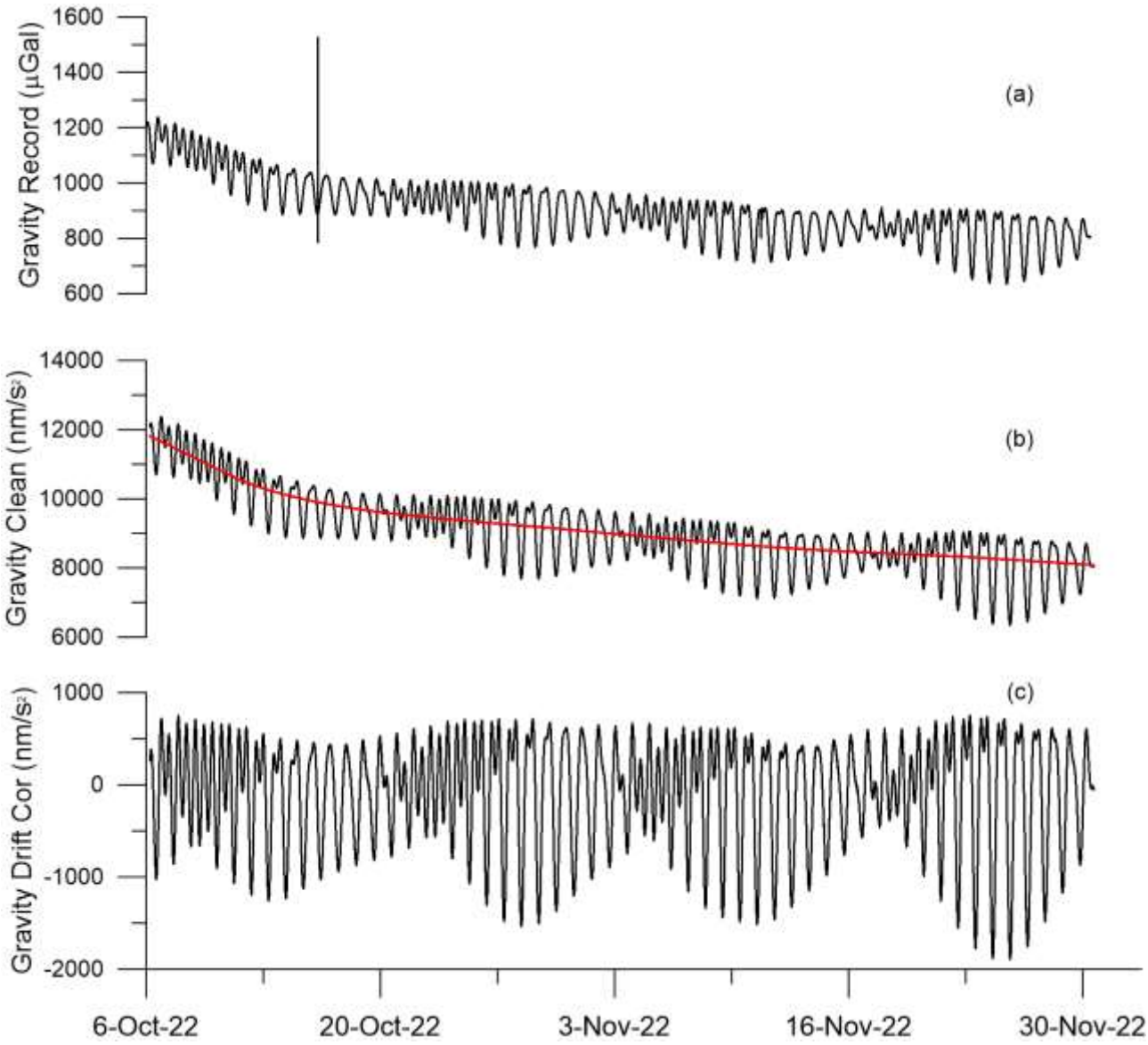

Fig. 3 *60 s gravity record collected at J9 Observatory with gPhonex#116 to prepare for tidal analyses: raw data (a), cleaned data (b), drift-corrected record (c); red curve is the modelled instrumental drift (3rd-order polynomial). .*

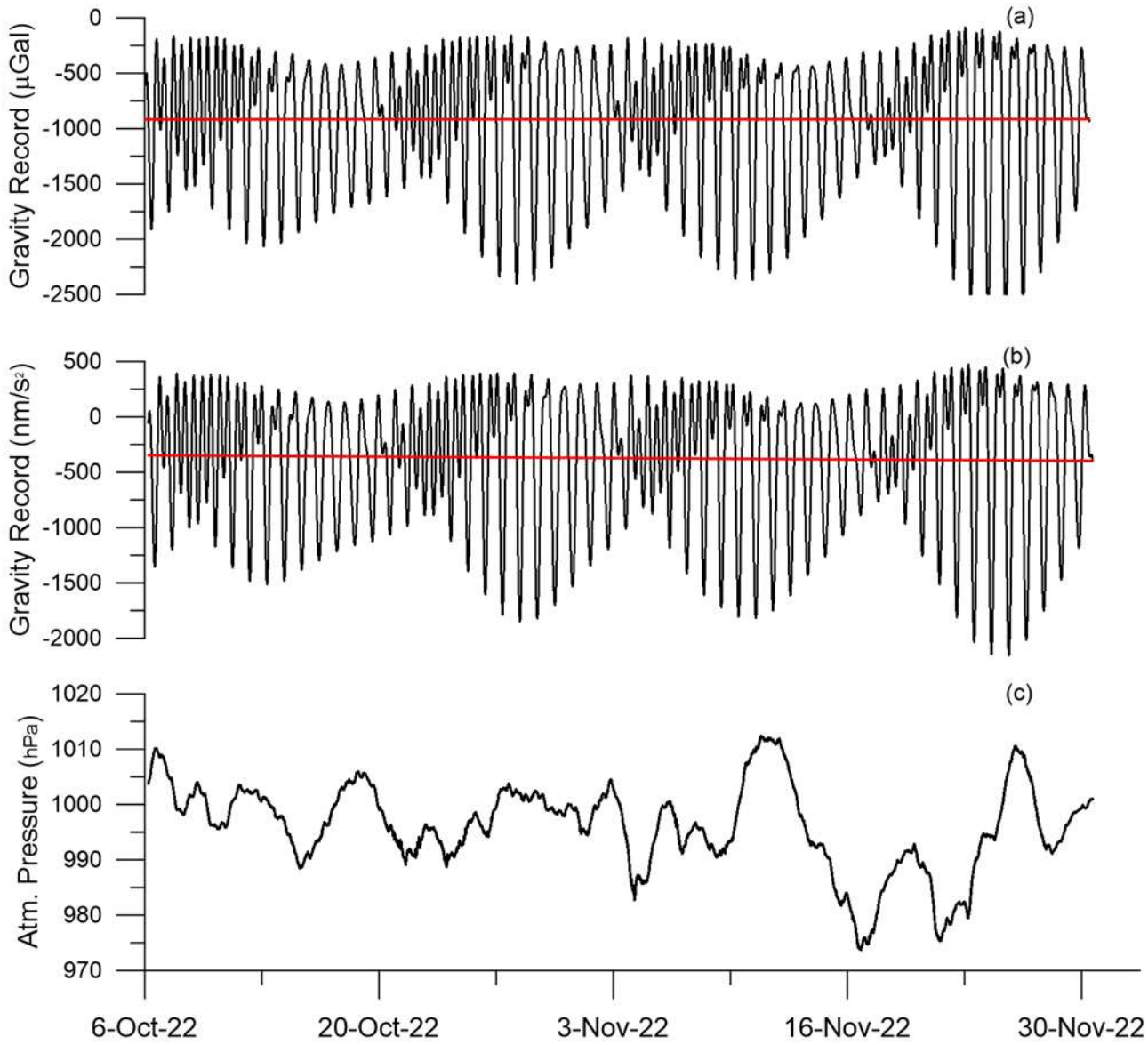

Fig. 4 *60 s records acquired at J9 Observatory: gravity collected with iOSG#023 (a) and iGrav#029 (b), atmospheric pressure (c); red curve is the modelled instrumental drift (linear fit).*

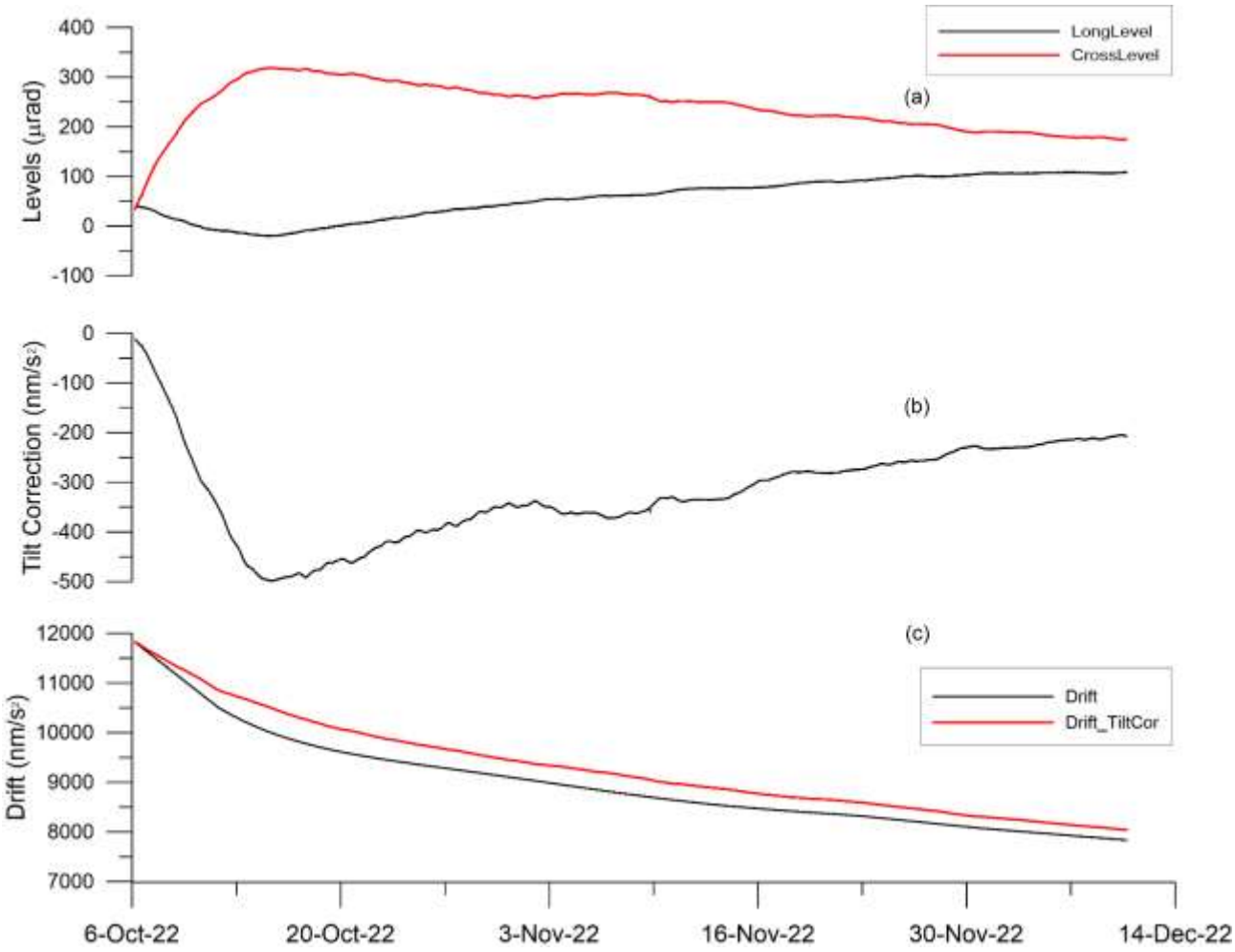

Fig. 5 *Effects of time variable tilt on drift: Recorded tilt (a); computed gravity effect due to tilt (b); 3rd-order polynomial instrumental drift with and without tilt correction (c).*

3.2 J9 Experiment: Absolute calibration of gPh#116 by FG5#2016 Absolute gravimeter

An absolute calibration was also carried out at J9 thanks to a 5-day recording session performed with the FG5#206 ballistic absolute gravimeter. The absolute measurements, conducted from 24 to 29 October 2022, provided a 30-second data set decimated to hourly values. To make the gPhone#116 pre-processed and drift-corrected signals comparable with the absolute data (Fig. 6a), they were further decimated from 60 s to 3600 s through a least-squares low-pass filtering with cut-off frequency of 12 cycle per day (cpd) and window half-length 480 samples (8 hours); the atmospheric pressure effects are reduced by means of the retrieved admittance factor -2.8 nms^{-2}/hPa.

In that case the scale factor with its statistical uncertainty is retrieved from the least-square simple linear regression of FG5#206 data versus gPh#116 ones (Figs. 6a, 6b); the FG5 drop standard deviations are accounted for in the fitting process.

As an alternative calibration approach, the synthetic tidal signal can be used too (Riccardi et al., 2011; Riccardi et al., 2023). When an accurate tidal model is available for a specific station derived from previous tidal analyses of long gravity recordings, as it is the case for J9 Observatory (Calvo et al., 2016), this synthetic signal can be used as a reference to validate the amplitude and phase response of any gravimeter collecting tidal observations in the same site. After correcting

gPh#116 for the atmospheric pressure effects as described before, a moving window regression (MWR) analyses is applied with respect to the synthetic tidal signal available for J9; the length of the MWR window was set to 5 days (7200 samples at one minute) in order to be comparable with the absolute calibration. This procedure allows to study the well-known time change of sensitivity that degrades the performance of spring gravimeters. This peculiar behaviour (Fig. 6c) could be partly due to the inaccuracy of tilt corrections when the recording spring gravimeters are not installed on levelling platforms and partly due to the inaccuracy of the drift modelling. Figure 6c provides an overview of the different calibration approaches adopted in this experiment.

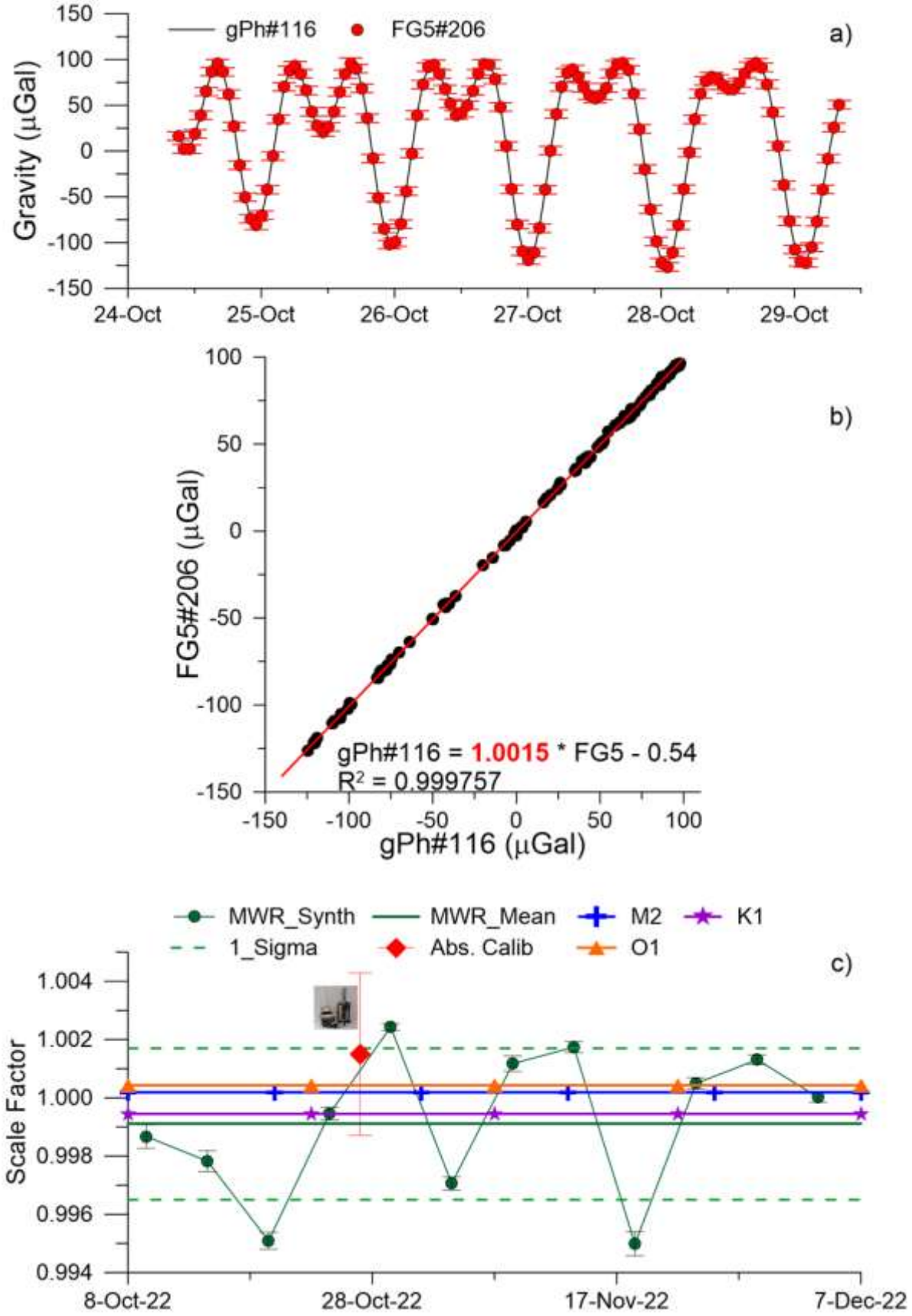

Fig. 6 *FG5#206 and gPh#116 gravity records collected during 5 days (a); absolute calibration of the gPh#116 (b); overview of all the calibration approaches used in this study including a moving window regression (MWR) analysis of gPh#116 versus synthetic tide (MWR Synth) (c). Tidal wave symbols (M2, K1, O1) indicate the relative calibration derived from the δ-Ratio with respect to iOSG#023; 1_sigma stands for 1σ standard deviation of MWR values*

3.3 Seismic noise and self noise levels

Some past studies have shown that the performance of mechanical gravimeters in terms of noise level was much poorer than the ones from SGs (Riccardi et al. 2011, Rosat et al. 2015). A characterization of the performance of the new generation of gPhoneX in terms of noise level is then necessary. With one instrument at a site, it is not possible to distinguish instrumental noise from the environmental noise. Since the gPh#116 is collocated with two SGs at J9, we safely assume that they record the same environmental noise in the same time-period. We then interpret the difference in the power spectral densities (PSDs) as instrumental, keeping in mind that at frequencies larger than 20 mHz, the oceanic seismic noise will have a different amplitude if the time-periods considered are different. We use the standard procedure that was first proposed by Banka (1997) and Banka and Crossley (1999) and applied to worldwide SGs by Rosat et al. (2004) and Rosat and Hinderer (2011). This procedure consists of computing the mean PSD of the 5 quietest days selected within the available time-records. The 5 quiet days are selected from the raw gravity data that were calibrated and reduced from solid tides and atmospheric pressure effect but not correcting for any disturbance like spikes or offsets (see Rosat et al. 2004 for details). This selection is based on the criteria of the lowest root-mean-square of residuals. We calculate the PSD using the robust Welch's superimposed segment mean estimator. We represent the PSDs with respect to the seismological New Low Noise Model (NLNM) of Peterson (1993), as a reference. The PSDs on the 5 quietest days for all kinds of relative gravimeters that recorded at J9 are plotted on Fig. 7. The 5 quietest days for the SGs iOSG#023, iGrav#029 and for gPh#116 were selected among the same time-period. For other relative mechanical gravimeters (ET-11, gPhone#054, Graviton, CG5), the 5 quietest days were selected on different time-periods since they were not recorded any more but corresponding to the one used in Rosat et al. (2015).

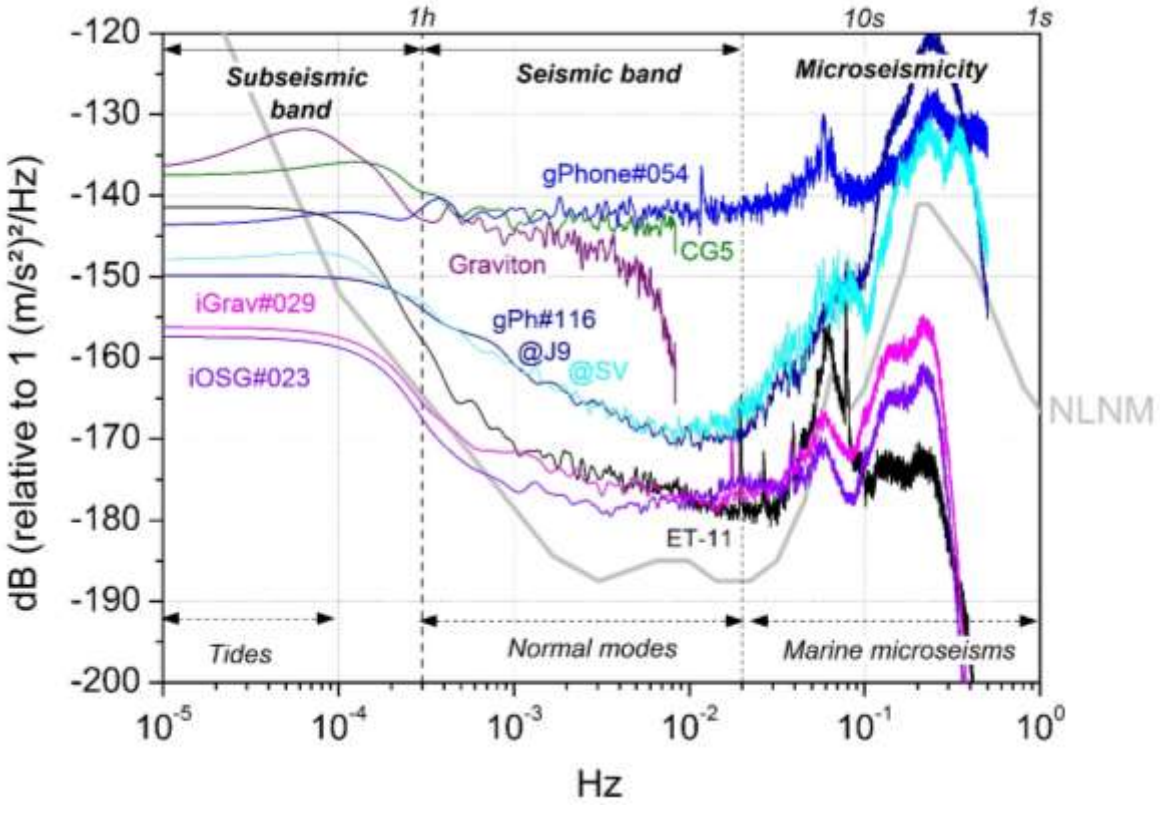

Fig. 7 *Fifth percentile of PSD noise levels computed on 1-s sampling data of gPh#116 collected both at J9 (dark blue curve) and SV station (cyan curve), the two SGs (iOSG23, iGrav29) and other spring gravimeters that have recorded at the J9 Gravimetric Observatory. The New Low Noise model (NLNM) of Peterson (1993) is represented by the thick gray line.*

Regarding the noise levels, as expected, the two SGs exhibit lower levels than gPh#116, in all spectral bands (Fig. 7). In the seismic band the noise levels of the two SGs appear in good agreement, within a few dB. As mentioned in Hinderer et al. (2022), this demonstrates that the various pillars at J9 do not significantly affect the noise level of the instruments. It is interesting to point out that gPh#116 exhibits lower levels at hourly time-scales than the other spring gravimeters (Graviton, gPhone#054, Scintrex CG5, L&R ET11). Compared to a similar instrument (gPhone#054) owned by the Spanish IGN, the gPh#116 also shows significantly lower noise levels with the exception of the seismic band (> 0.1 Hz). In the normal mode band, the best spring gravimeter is the old LaCoste & Romberg Earth Tide gravimeters (L&R ET11). At the high frequency end of the spectrum there is a steep roll-off, namely a slump in amplitude, till the Nyquist frequency of 0.5 Hz because of the built-in low pass anti-aliasing filters of the SGs and the gPhoneX gravimeters. The roll-off of the Graviton at $f > 10^{-2}$ Hz is due to the unavailability of data sampled at 1 Hz. (see Rosat et al., 2015 for details). While the gPh#116 is about 10 dB noisier (a factor ~3 in amplitude) than the SGs at seismic frequencies, the instrumental improvement of the gPhoneX is conspicuous. It is 10 dB less noisy than the gPhone#054 at 1 h and 20 dB less noisy at 20 mHz. We have also computed the mean PSD of the 5 quietest days for the gPh#116 when recording at Mt Somma-Vesuvius (Fig. 7, @SV). The observed noise level is similar to the one at J9, except for the microseismic noise, the latter depending strongly on the time-period of the recording and the location. Assuming the instrumental gPh#116 noise was not modified during transportation, it means the environmental noise at Mt Somma-Vesuvius is similar to the one at J9 in the seismic frequency range considered here.

The parallel records at J9 of gPh#116, iOSG#023 and iGrav#029 also gave us the opportunity for a three channel correlation analysis (Sleeman et al., 2006) to extract the incoherent contributions of the three gravimeters from the coherent ones. Such an analysis is an efficient tool to separate environmental noise (common noise coherent between the 3 instruments) from the assumed instrumental noise (the so-called self-noise, which is incoherent between the instruments). Figure 8b shows the PSD plot of the self-noise computed according to Sleeman method on raw calibrated data (i.e. data are not corrected at all, so they contain tides as well as all other environmental effects). Self-noise was extracted on October 12, 2022, one of the quietest day at J9 for gPh116. Some other quiet days show same self-noise features. The observed PSD noise, that is the one which contains all effects, is plotted too (Fig. 8a).

The main results of the application of the Sleeman test show that the method is not as efficient as when applied on three SGs (see Rosat & Hinderer 2018) to separate environmental from instrumental noise, since the PSDs do not get flat towards low frequencies, meaning that the recorded tides between gPh#116 and SGs are not as coherent as they should be (Fig. 8c). This could be due to the non-linear drift terms in the spring meter. It also turns out clearly that the iOSG23 has a low-pass filter which cuts at lower frequency than the iGrav29's one, while the gPh116 does not seem to have any sharp low-pass filtering since there is no clear decrease at high frequencies. There is a loss of coherency between both SGs between 20 and 100 mHz, which is the frequency range where the resonance modes of the levitating spheres are; that was also observed for other instruments at J9 (Rosat et al. 2015).

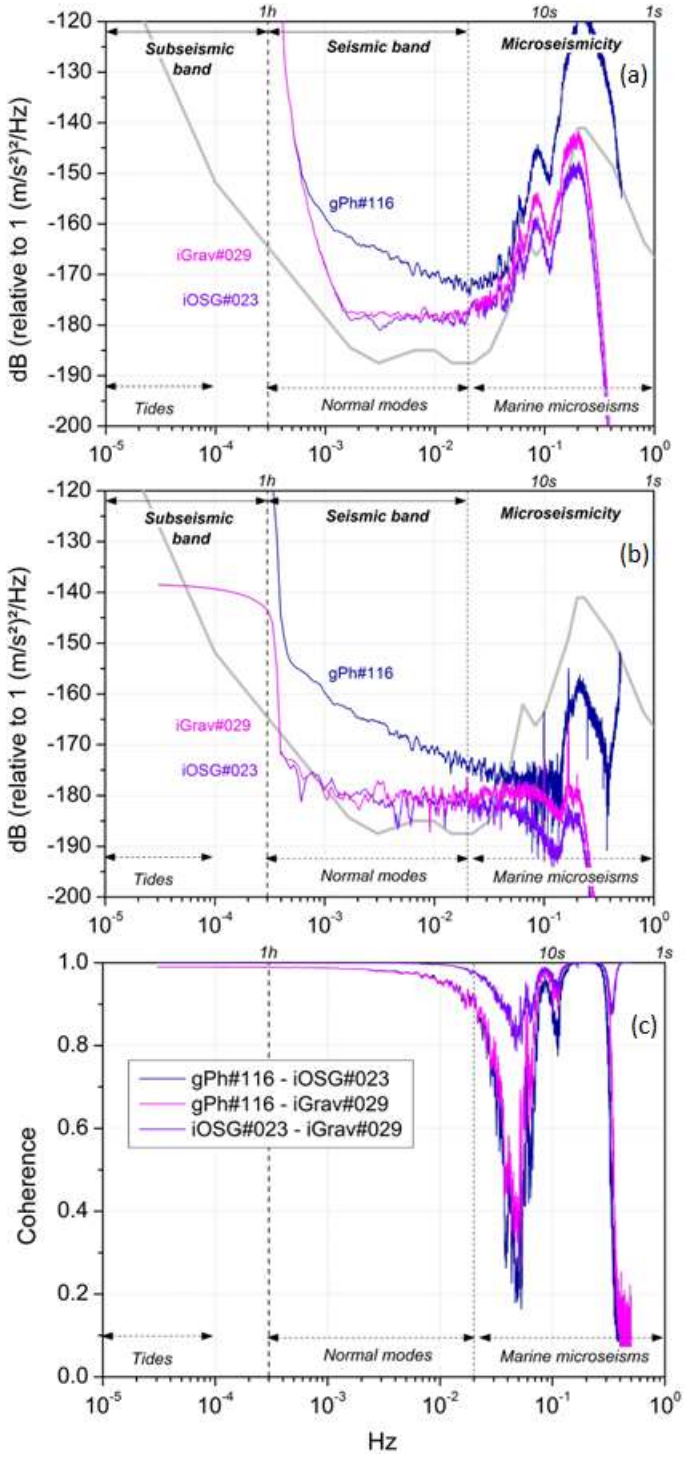

Fig. 8 *Three channel correlation analysis applied to parallel records of gPh#116, iOSG#023 and iGrav#029 collected during one of the quietest days at J9 for gPh116 (October 12, 2022): observed PSD noise (a); self-noise (b) and coherence (c).*

As a final step in assessing the instrumental performance of gPh#116, the residual gravimetric signals are compared (Fig. 9); gravity residuals are obtained after adjusting the observed tide at J9 and atmospheric pressure by means of ET34-X-V80; these results are discussed with more details in the following section 4.

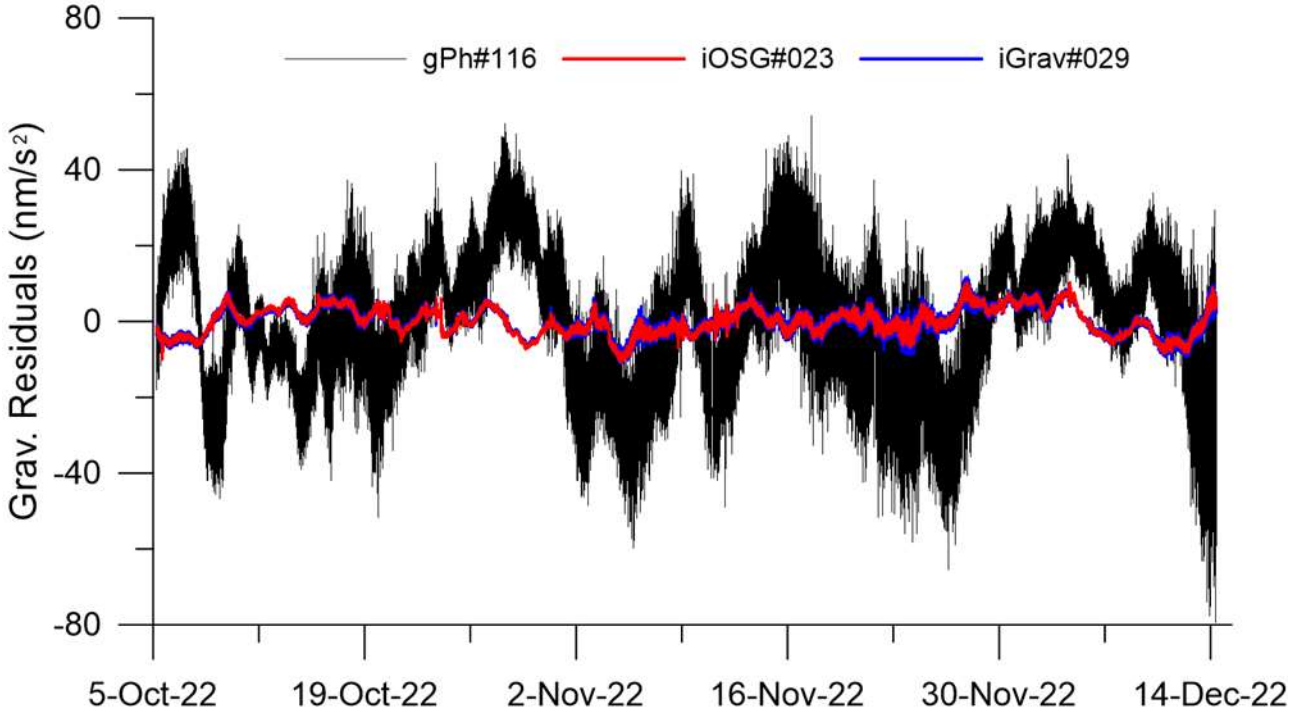

Fig. 9 *1-min gravity residuals obtained with ET34-X-V80 code for gPh#116 and the two SGs co-located at J9.*

3.4 Gravity records at Mt. Vesuvius station (Tidal model and Residuals)

275 days of gravity records spanning 29 December 2021 – 29 September 2022 were collected at SV (Fig. 10b). Various issues have occurred during the acquisition interval, leading to a rather discontinuous database, characterised by long interruptions, such as the one encompassing 12 January - 1 April due to a UPS failure and from 20 May to 7 June due to an electrical problem, and other gaps of shorter duration (Fig. 10b, c). Out of the gaps, about 178 net days of gravity recording were available (about 65% of the time span). Due to such a discontinuous observation period and frequent adjustment of the tilts, any significant drift study was possible, except for studying the effect of the multiple stop & starts of the gravimeter. This is why more in-depth study on the drift have been done during the J9 experiment (see § 3.1). Same pre-processing, as described for J9 experiment, are applied to 1Hz sampled data (Fig. 10a). It is quite evident that the long-term trend of the record systematically displays a large amplitude and non-linear gravity changes (Fig. 10b) eventually due to the relaxation of the spring consequent to the restart of the gravimeter, as mentioned in the § 3.1. On the pre-processed 60 s recordings of both gravity and atmospheric pressure a tidal analysis is performed by means of ET34-X-V80 (Schüller, 2020). Given the length (< 6 months) of the analysed gravity time series, the results [delta (δ) & phase (φ)] for the resolvable wave groups are listed in Table S2. The quality of the tidal model was assessed through various benchmarks and compared with previous similar determinations (Tab. 2). After adjusting for body tides, atmospheric and polar motion effects with ET34-X-V80, the gravity residuals are obtained (Fig. 10d). The ambient pressure admittance is also recovered from the least-squares linear regression of gravity residuals versus atmospheric pressure. These findings are described in detail and discussed in section 4 "Discussion".

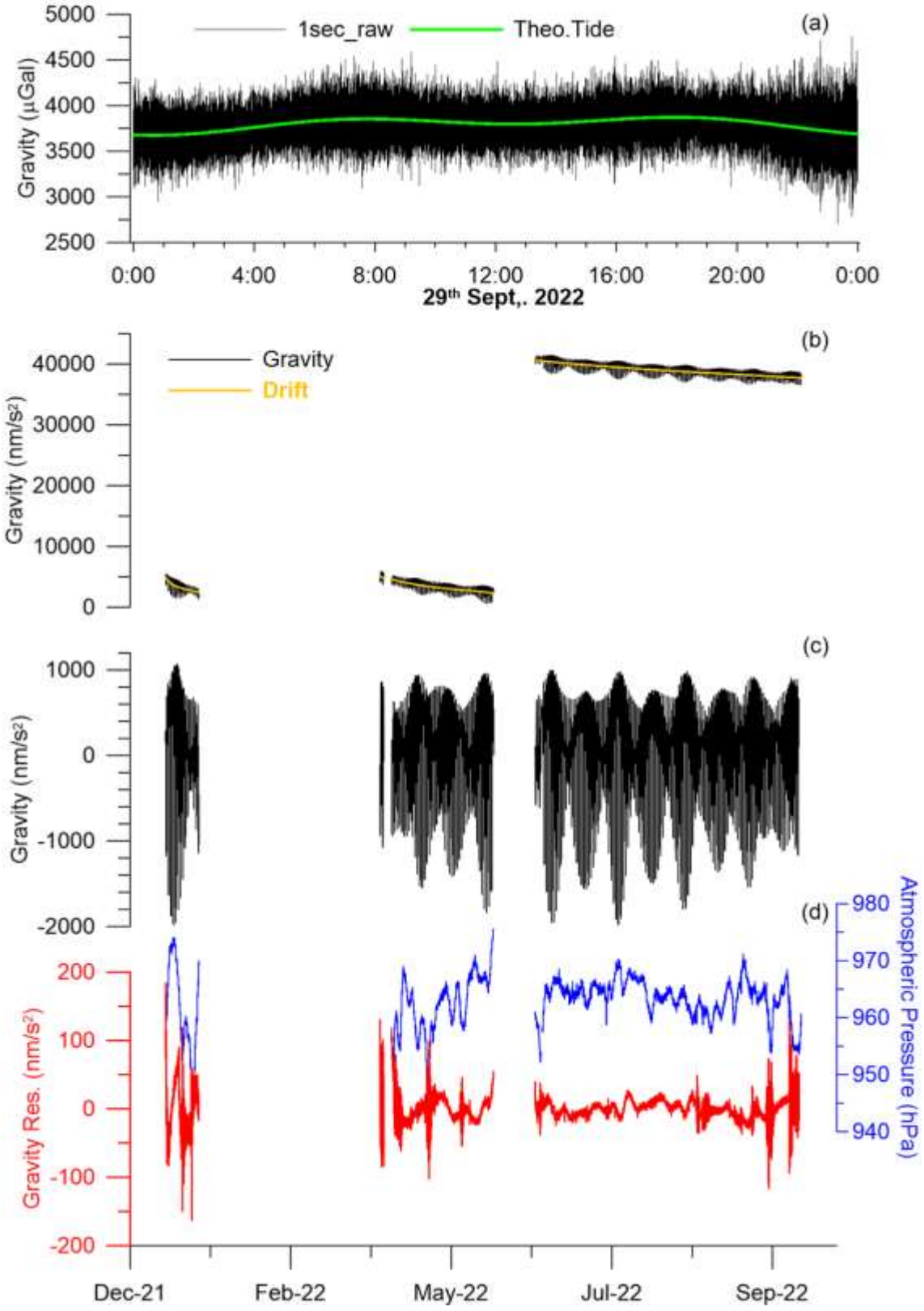

Fig. 10 *Gravity records collected with the gPh#116 at the Mt. Somma-Vesuvius permanent gravity station between December 2021 and September 2022: Example of 1 s raw gravity record (1 day long) with theoretical tide(a); 60s gravity data with the modelled drift (b); drift corrected gravity (c); gravity residuals after adjusting tides and pressure effect with ET34-X-V80 and atmospheric pressure (d).*

4 Discussion

The synoptic picture of the calibration results (Fig. 6c), obtained with different techniques, shows a certain discrepancy between the results and furthermore it is evident that the precision of the absolute calibration is less than that recoverable from the tidal analyses compared with those of the superconducting gravimeters. This is not surprising at all, in fact, and it was demonstrated in previous studies (e.g. Calvo et al., 2014; Hinderer et al., 2022) that the internal stability of the SGs (about 0.1%), derived from tidal analyses, is at least an order of magnitude greater than the stability that can be achieved with repeated calibrations with an absolute gravimeter. Indeed, absolute gravity measurements are affected by a noise level higher than SGs (Rosat et al. 2015) which limits the accuracy of the retrieved scale factors. In principle, having a superconducting gravimeter with an accurate calibration, it is possible to estimate the scale factors of other relative gravimeters by co-locating them and comparing the joint records (e.g. Meurers 2002, Riccardi et al. 2012). It is acknowledged that SGs are extremely precise and stable relative gravimeters, therefore a relative calibration can never be more accurate than the calibration of the instrument used for calibration; we will get a very precise calibration, but not as accurate.

The intercomparison experiment conducted at J9 shed light on the instrumental drift behaviour already observed by other authors. The gPh#116 presents a strongly non-linear drift that could be attributed to the initial relaxation of the spring that persists for the first 10-15 days and then becomes linear with slopes of at least an order of magnitude smaller. A contribution to the instrumental drift comes from the time variation of the uncompensated ground inclination and thus with loss of verticality by the instrument (Fig. 5c). The multiple calibration approaches used made it possible to verify that the calibration constant provided by the manufacturer was reliable at a level of accuracy of 0.1%.

Even applying the tilt correction, the biggest differences between the gPh#116 and the SGs look incoherent (Fig. 9), with much larger residuals for gPh#116. Compared to the SGs 60s residuals, the gPh#116 residuals are much more scattered with 100 nm s^{-2} peak-to-peak and a standard deviation (SD) of 16.6 nm s^{-2}. The SG residuals are between −11 and 10 nm s^{-2} (21 nm s^{-2} peak-to-peak) with a SD of 3.7 nm s^{-2}. The linear correlation coefficient between the residuals from the two SGs is 0.9968 while that from gPh#116 with respect to the iOSG#023 is only 0.23. Having in mind that a time correlation covers all frequency bands, this is not surprising in view of the imperfect frequency coherency obtained between uncorrected data (Fig. 8c).

Accounting for the length of the available gravity recording collected on Mt Somma-Vesuvius (178 days), 30 tidal groups are reliably retrieved (Tab. S2) in terms of tidal parameters (delta-δ and phase-φ). Unfortunately, due to the limited length of the recording, it was not possible to resolve some individual tidal waves, which are relevant for the latitude of the site, in the diurnal tidal band (e.g. S1K1). Indeed, as the recording period encompasses nearly 9 months, a 6-month spectral separation can be safely used, which allows to split the P1S1K1 group into P1 and S1K1 sub-groups as well as S2K2 into S2 and K2. Results for the main resolved tidal waves are listed in Table 2 and compared with previous determinations using the LCR-D126 (Riccardi et al. 2008).

Table 2 *Comparison of the delta factors for the four main tidal waves determined at Mt. Somma-Vesuvius in the present study with gPh#116 and previous studies with LCR-D126. Notice that K1 is not fully comparable with previous determinations, because it is currently not separable from S1 in the diurnal tide band. In addition, deltas for P1 and K2 waves are not compared because they are unpublished; *parameters from Riccardi et al. (2008).*

	Delta factors		
Wave	**1994-1998***	**1999-2000***	**Present study**
O1	1.126 ± 0.002	1.143 ± 0.004	1.1478 ± 0.0001
K1	1.117 ± 0.001	1.123 ± 0.003	1.1353 ± 0.0001

M2	1.1488 ± 0.0007	1.155 ± 0.001	1.17823 ± 0.00007
S2	1.144 ± 0.004	1.155 ± 0.003	1.1746 ± 0.00015

The delta factors obtained differ significantly from those determined in the past, far beyond the errors reported by the authors. This shows that the LCR-D126 gravimeter had calibration problems that were not solved even by intercomparison with an SG at the Brasimone station, where the operating SG TT70-T015 itself had some calibration problems (Baker & Bos, 2003).

To assess the quality of the retrieved tidal model some proxies can be used. For example, the amplitude ratio δM2/δO1 is acknowledged to be not depending on calibration inaccuracies and is therefore useful for assessing how well observed deltas and those reduced by ocean loading match a given Earth model. The results are compared with the ones expected by the most recent tidal models (Tab. 3): the hydrostatic, elastic Earth (DDW-H), the non-hydrostatic, inelastic Earth (DDW-NHi) (Dehant et al., 1999) and the non-hydrostatic, inelastic Earth model (WDZ-NHi) (Dehant & Zschau, 1989; Wahr & Bergen, 1986).

Tab. 3 *Amplitude ratio δM2/δO1; see the main text for the listed Earth models*

Model	Theoretical	Observed
DDW-H	1.00662	1.0084±0.0001
DDW-NHi	1.00663	
WDZ-Hi	1.00352	

Again in order to provide a benchmark on the quality of the assessed tidal parameters at a glance, the delta factor for the 6 main tidal waves for Mt Somma-Vesuvius area are plotted in Fig. 10 together with their ocean tidal loading (OTL) corrections according to the FES2014b model (Carrere et al., 2015). It is clear that, at least for the main waves, FES2014b suitably reproduces the oceanic effect. The final residual X-vectors (refer to Fig 11c for the used convention) are all < 1 % (Fig. 11b; refer to Fig. 11c for the notation). Other recent OTL models have been tested too, like EOT20, CSR4.0, TPXO.95c, GOT4.10c, freely available on the web at the OTL provider (Bos & Scherneck, 2023); negligible differences are retrieved.

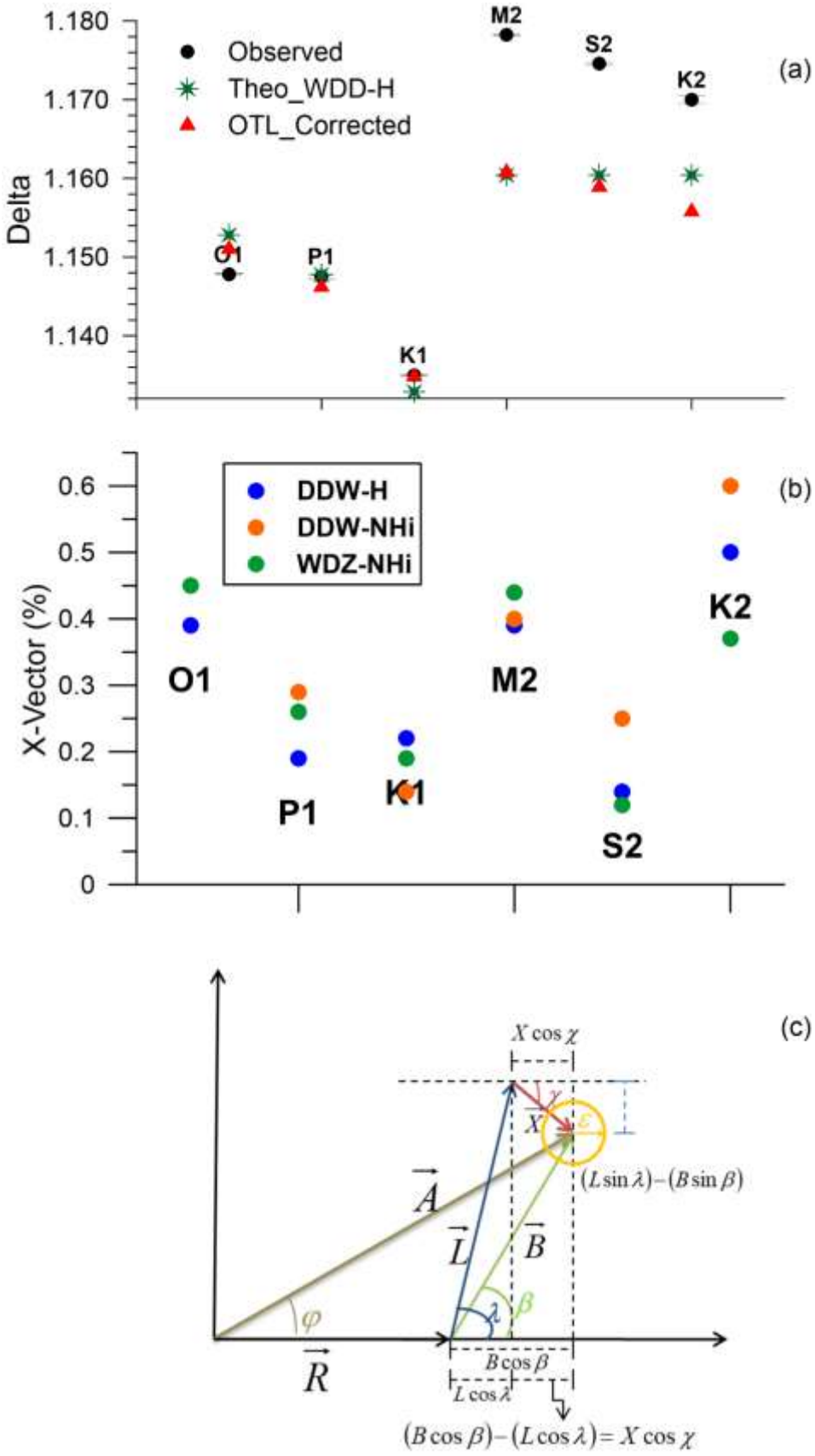

Fig. 11 *Diurnal and semi-diurnal tidal factors and ocean tide loading (OTL) correction. (a) Observed and OTL-corrected delta factors ; (b) final residual OTL vector X for the 6 main tidal waves in percentage wrt R (|**X**|/|**R**|*100); (c) convention of vector representation of Earth tide and ocean loading : R=Earth model tidal amplitude, A=observed tidal amplitude, L=OTL vector according to a specific model.*

A barometric admittance of -3.6 ± 0.1 nm/s²/hPa was retrieved by the simultaneous least squares fit in ET34-X-V80 with the ambient pressure recordings.

1-min gravity residuals obtained after reducing the instrumental drift and geophysical effects (observed body and oceanic tides, polar motion, atmospheric pressure) exhibit a level of high-frequency noise that appears to correlate well with atmospheric pressure minima (Fig. 10d). We believe that this high-frequency disturbance is likely related to the weather conditions, especially the wind effects on the pine forest above the underground laboratory. Gravity residuals decimated to 3600s fluctuate between ±25 nm/s^2 with standard deviation of 14 nm/s^2. It is very likely that the small fluctuations remaining on the residual signal after the best tide adjustment are related mainly to uncorrected drift components; this is supported by the analysis of SG and gPhone at Strasbourg, where no clear correlation between the residuals of the instruments is observed (Fig. 9).. This comparison also rules out the possibility of detecting transient hydrological components at the temporal scale of few weeks at the Vesuvius with the gPhone, at least with such instrument which is not equipped with a proper tilt compensation system.

In any case, on the temporal scale of few days, the gPhone may be helpful in unveiling and characterizing the short-term hydrological recharge processes. The geological situation of the SV underground laboratory is such that above the gravimeter room there is a soil cover due to the weathering of loose pyroclastic products from the SV's explosive and Strombolian activities. This soil has been colonized by a dense pine forest. In the dry season, autumn rainfall peaks predominantly soak the surface layers of the soil above the gPh#116, therefore a negative gravity change is expected. We have tried to quantify this effect by selecting the largest rain event during the recording period that occurred on September 25th 2022 (cyan rectangle in Fig. 12b). Rain data have been collected at Ercolano station (Fig. 1) managed by the Civil Protection (http://centrofunzionale.regione.campania.it/#/pages/sensori/sensor-utility) about 2 km away from the gPh#116. The available rain data, sampled at 600 s (10 min), were converted in hourly values and compared with gravity residuals (Figs. 12b). In order to assess the amount of rain soaking the soil the cumulated rain is computed (Fig. 13a). Actually a gravity decrease of about 5 nm/s^2 seems to be observed on the occasion of the largest rain peak (about 30 mm). An empirical rain admittance is retrieved from the scatter plot of gravity versus the cumulated rain (Fig. 13b). Notwithstanding the poor correlation, the retrieved rain function seems to work fine in accounting for the small induced gravity effect. This appears from both the visual inspection of the corrected time series (Fig. 13c) as well as from the lowering of the rms of the corrected gravity residuals that drops down from 4 to 2 nm/s^2. The retrieved admittance value amounting to -0.049 ± 0.004 nms^{-2}/mm is significantly lower than the standard value of -0.42 nms^{-2}/mm of the infinite Bouguer slab (Torge, 1989). Based on a statistics of about 30 rain events, Hector et al. (2014) retrieved a rainfall admittance for an SG station in Djougou (Benin-West Africa). Even in that case they found values lower than the classical Bouguer effect, that were explained as due to the shelter mask along with evapotranspiration. In our case a number of further factors may contribute to lower the absolute admittance value, namely the runoff draining out the water together with the local effect due to topography (Meurers et al., 2007), the evapotranspiration of the pine forest as well as the umbrella effect cannot be ruled out.

A more quantitative modelling would require the selection of a statistically significant number of hydrological transients that were not available due to the very short time series analyzed in this study.

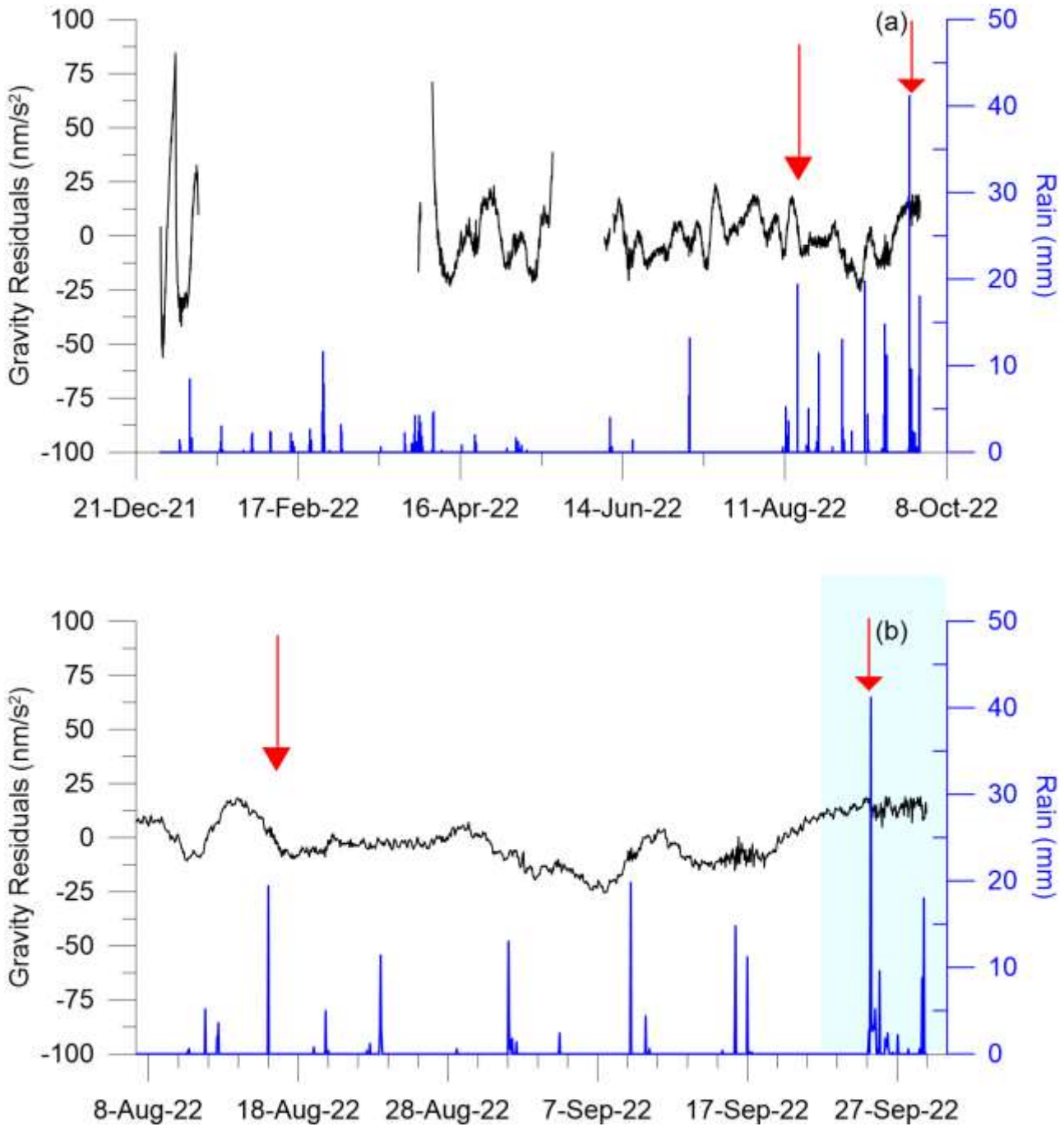

Fig. 12 *Gravity and rainfall records at Mt. Somma-Vesuvius: (a) hourly gravity residuals after adjusting gravity tides (black curve) and cumulated rain (blue curve); (b) zoom into the end of the dry season (summer); the red arrows mark the occurrence of rain events at SV; the cyan rectangle highlights a time span with heavy rain discussed in the main text (see Fig. 13).*

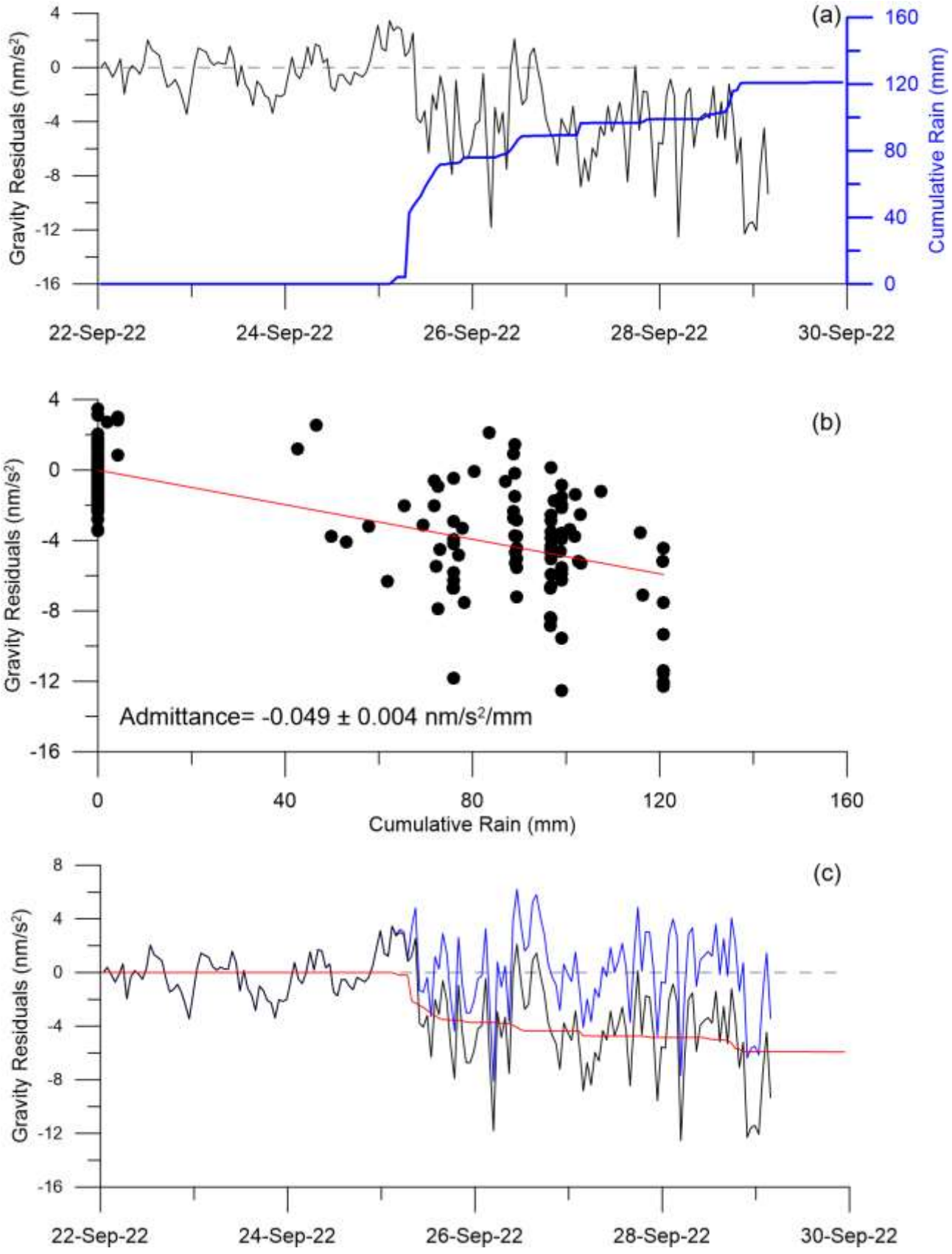

***Fig. 13**: Rain gravity effect at the gPh#116 station due to the rain fall event of 25th September 2022: (a) gravity residuals and cumulated rain; (b) scatter plot of gravity vs. cumulated rain and the linear best fit to retrieve the admittance coefficient; (c) Rain gravity effect computed from the admittance (red line) together with uncorrected (black) and corrected (blue) residuals.*

The influence of some possible local effects at the SV station is evident from the appearance of a clear inverse correlation between the transverse level signal and the ambient pressure (Fig. 14) with an admittance factor of -0.15± 0.05 μrad/hPa. As this correlation was not found during the intercomparison experiment at J9, we think it could be related to a kind of cavity effect, due to the geometry and orientation of the underground laboratory structure, which would respond elastically in a peculiar way to the passage of atmospheric pressure fronts. However, this phenomenon could not be analyzed quantitatively in this study, but would be worth investigating in a future specific study by exploring for instance the response to the atmospheric waves generated by the violent eruption of Hunga Tonga volcano on January 15, 2022 (e.g. Wright et al. 2022).

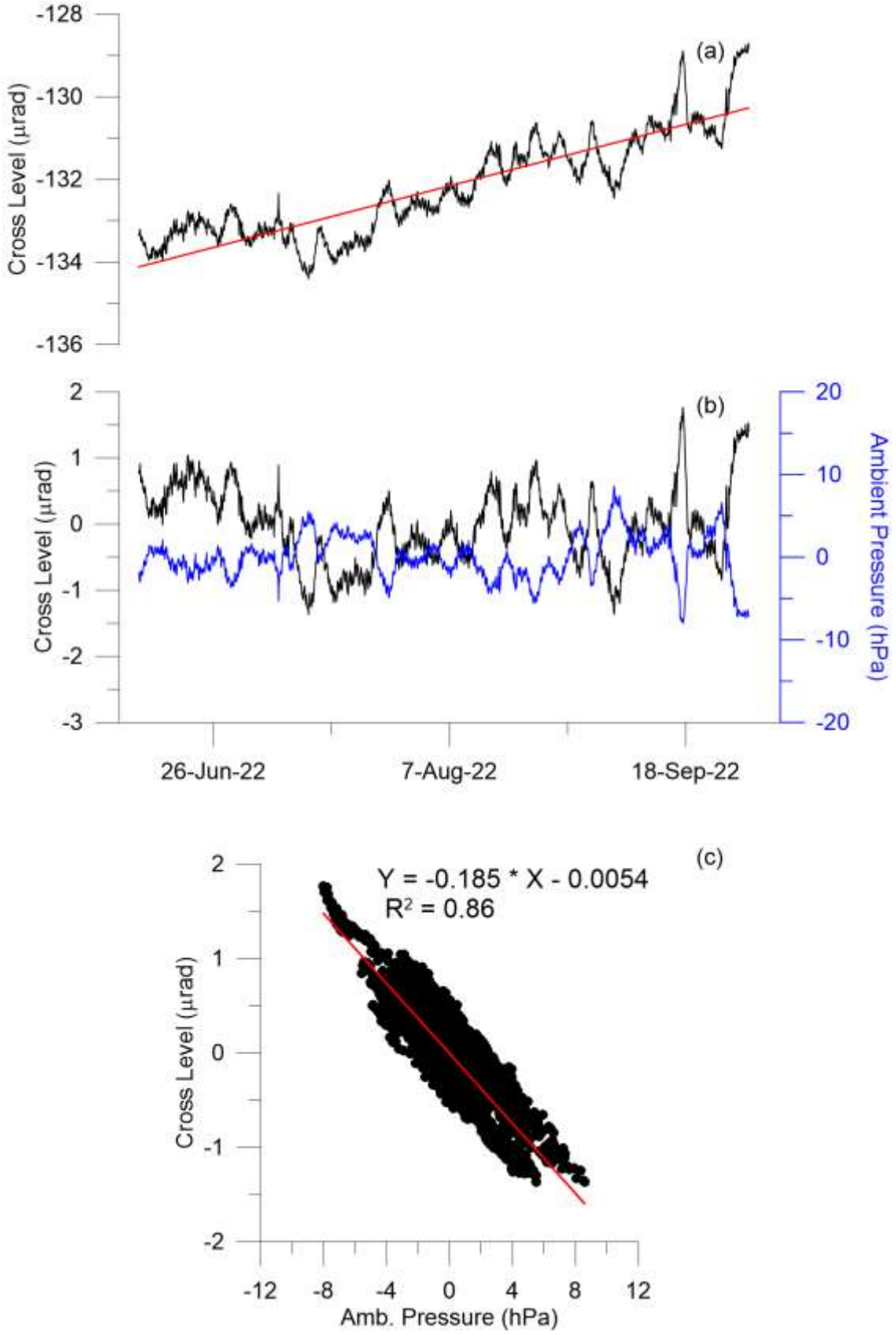

Fig. 14 *Tilt and atmospheric pressure records by the gPh#116 at Mt. Somma Vesuvius station: (a) Hourly values of the tilt changes measured by the cross level; (b) de-trended cross level and ambient pressure signals; (c) Linear regression of tilt changes vs. Pressure, statistics of the fitting is given too.*

5 Conclusions

About 6 months (178 days) of continuous gravity recording were collected on Mt Somma-Vesuvius with the new generation gPhoneX gravimeter enabling us to achieve a more reliable tidal model than previous attempts produced in the 1990s with the LCR-D126 land gravimeter. Furthermore, in order to study the instrumental response of the gPhone#116 in great detail, an intercomparison experiment was conducted at the J9 gravimetric observatory in Strasbourg, where several superconducting gravimeters operate permanently. The gPhoneX116 has been calibrated with respect to two superconducting gravimeters and an absolute gravimeter FG5. On that occasion the noise level was checked and compared with other spring gravimeters. While it was not possible to carry out an accurate study of the instrumental drift of gPh#116 during the approximately 9 months of recording at Vesuvius, due to the frequent interruptions of the recordings, which sometimes lasted several months, leading to the compilation of a very inhomogeneous database of records, this was possible during the intercomparison experiment conducted at the J9 observatory. During the intercomparison, the gravimeter showed a peculiar behaviour already highlighted by other authors in similar experiments. In particular, the acquired gravimetric recordings showed a typical drift pattern that was very strong in the first 10-15 days after installation and then reduced in amplitude, becoming linear. A non-negligible part of the instrumental drift, or it would be more correct to call it the long-term behaviour, is attributable to the instrumental response to changes in ground tilt. The main conclusion of the J9 experiment is that the multiple calibration approaches lead us to validate the calibration constant provided by the manufacturer at a level of accuracy better than 1 % and precision of 0.1%. However, a negative aspect that has emerged from this experience is that, even when tilt correction is applied, the gravimetric residuals recoverable from gPh#116 appear much larger (at least an order of magnitude) and completely out of line with those obtained with collocated superconducting gravimeters; this would claim the need to acquire a self-levelling platform.

The small amplitude gravity residuals (±20 nm/s^2 = 2 μGal) obtained at SV station appear to be mainly influenced by an uncorrected short-term drift component. In some occasions, in particular at the end of the dry summer season the first rainfalls seem to produce rapid gravity decreases due to the soil moisture above the underground laboratory hosting the gPh#116. The observed gravity signal is smaller than the predicted Bouguer slab because of the significant runoff and the steep topography. Unfortunately, the limited time span (9 discontinuous months), with few intense rain events doesn't allow a reliable study of such short-term recharge processes. Indeed characterizing such signals at Vesuvius would be important, especially for the time-lapse gravity campaigns performed for the volcano monitoring.

A clear inverse correlation between the gPh#116 cross level signal and atmospheric pressure was revealed at the Mt. Somma-Vesuvius underground laboratory, which would likely represent a cavity effect related to the geometry of the laboratory. Further study is however necessary to confirm such a cavity effect.

Acknowledgments: This research was partially funded by the Agreement between Istituto Nazionale di Geofisica e Vulcanologia and the Italian Presidenza del Consiglio dei Ministri, Dipartimento della Protezione Civile (DPC).

References

Baker, T.F., Bos, M. (2003). Validating Earth and ocean tide models using tidal gravity measurements, *Geophys. J. Int.*, *152, 468–485*.

Baldi, P., Casula, G., Hinderer, J., and Amalvict, M. (1999). Calibration of a superconducting gravimeter: a comparison between the mass sttraction method and the use of FG5 absolute gravity measurements, *Boll. Geofisica Geodetica*, *40* (2-3), 583-588.

Banka, D. (1997). *Noise levels of superconducting gravimeters at seismic frequencies, Ph.D. Thesis*, GDMB-Informationgesellschaft mbH, Clausthal, Germany.

Banka, D., and D. Crossley (1999). Noise levels of superconducting gravimeters at seismic frequencies, *Geophys. J. Int*. 139, 87-97.

Battaglia, M., Gottsmann, J., Carbone, D., & Fernández, J. (2008). 4D volcano gravimetry. *Geophysics*, 73(6), WA3-WA18. https://doi.org/10.1190/1.2977792.

Berrino, G., Corrado, G., Magliulo, R., Riccardi, U., 1997. Continuous record of the gravity changes at Mt. Vesuvius. *Ann. Geofis*. 40, 1019–1028.

Berrino, G., Cerutti, G., Corrado, G., De Maria, P., & Riccardi, U. (1999). Gravity studies on active Italian volcanoes: a comparison between absolute and relative gravimetry. *Boll. Geofis. Teor. Appl*, 40 (3-4), 497-510.

Berrino, G., 2000. Combined gravimetry in the observation of volcanic processes in Southern Italy. *J. Geodyn*. 30, 371– 388.

Berrino, G., Corrado G., Riccardi U. (2006): On the capability of recording gravity stations to detect signals coming from volcanic activity: The case of Vesuvius, *J. Volcanol. Geotherm. Res.*, 150, 270-282.

Berrino G, d'Errico V, Ricciardi G. Thirty years of precise gravity measurements at Mt. Vesuvius: an approach to detect underground mass movements (2013). *Ann. Geophys*.10; 56(4): S0436. Available from: https://www.annalsofgeophysics.eu/index.php/annals/article/view/6442.

Borgia, A., Tizzani, P., Solaro, G., Manzo, M., Casu, F., Luongo, G., ... & Lanari, R. (2005). Volcanic spreading of Vesuvius, a new paradigm for interpreting its volcanic activity. *Geophysical Research Letters*, *32*(3). https://doi.org/10.1029/2004GL022155.

Bos, M., & Scherneck, H-G. (2023). Free ocean tide loading provider. http://holt.oso.chalmers.se/loading/. Accessed 14 Jan 2023.

Caliro, S., Chiodini, G., Avino, R., Minopoli, C., & Bocchino, B. (2011). Long time-series of chemical and isotopic compositions of Vesuvius fumaroles: evidence for deep and shallow processes. *Annals of Geophysics*. http://hdl.handle.net/2122/7212.

Calvo, M., Hinderer, J., Rosat, S., Legros, H., Boy, J.-P., Ducarme, B., & Zürn, W. (2014). Time stability of spring and superconducting gravimeters through the analysis of very long gravity records. *Journal of Geodynamics*, 80, 20–33. https://doi.org/10.1016/j.jog.2014.04.009.

Calvo, M., Rosat, S., Hinderer, J. (2016). Tidal spectroscopy from a long record of superconducting gravimeters in Strasbourg (France). *International Associations of Geodesy Symposia, Prague* (Czech Rep.). Berlin, Heidelberg: Springer. https://doi.org/10.1007/1345_2016_223.

Carbone D., Poland M., Diament M., Freco F. (2017). The added value of time-variable microgravimetry to the understanding of how volcanoes work. *Earth-Science Reviews*, 169: 146-179. https://doi.org/10.1016/j.earscirev.2017.04.014.

Carlino, S. (2018). Heat flow and geothermal gradients of the Campania region (Southern Italy) and their relationship to volcanism and tectonics. *Journal of Volcanology and Geothermal Research*, *365*, 23-37. https://doi.org/10.1016/j.jvolgeores.2018.10.015.

Carrere, L., Lyard, F., & Cancet, M. (2015). *FES2014, a new tidal model on the global ocean with enhanced accuracy in shallow seas and in the arctic region*. EGU general assembly 2015 (pp. 12–17) April Vienna (Austria).

Cella, F., Fedi, M., Florio, G., Grimaldi, M., & Rapolla, A. (2007). Shallow structure of the Somma–Vesuvius volcano from 3D inversion of gravity data. *Journal of Volcanology and Geothermal Research*, *161*(4), 303-317.

Chiodini, G., Marini, L., & Russo, M. (2001). Geochemical evidence for the existence of high-temperature hydrothermal brines at Vesuvio volcano, Italy. *Geochimica et Cosmochimica Acta*, *65*(13), 2129-2147. https://doi.org/10.1016/S0016-7037(01)00583-X.

Crossley, D., Hinderer, J., & Riccardi, U. (2013). The measurement of surface gravity. *Reports on Progress in Physics*, 76, 046101. https://doi.org/10.1088/0034-4485/76/4/046101.

Cusano, P., Petrosino, S., Bianco, F., & Del Pezzo, E. (2013). The first Long Period earthquake detected in the background seismicity at Mt. Vesuvius. *Annals of Geophysics*. http://hdl.handle.net/2122/8832.

D'Auria, L., Massa, B., & Matteo, A. D. (2014). The stress field beneath a quiescent stratovolcano: The case of Mount Vesuvius. *Journal of Geophysical Research*: Solid Earth, 119(2), 1181-1199. https://doi.org/10.1002/2013JB010792.

Dehant, V., Defraigne, P., & Wahr, J. (1999). Tides for a convective Earth. Journal of Geophysical Research, 104(B1), 1035–1058.

Dehant, V., & Zschau, J. (1989). The effect of mantle inelasticity on tidal gravity: A comparison between the spherical and the elliptical Earth model. *Geophysical Journal International*, 97(3), 549–555. https://doi.org/10.1111/j.1365-246X.1989.tb00522.x.

De Martino P, Dolce M, Brandi G, Scarpato G, Tammaro U. (2021). The Ground Deformation History of the Neapolitan Volcanic Area (Campi Flegrei Caldera, Somma–Vesuvius Volcano, and Ischia Island) from 20 Years of Continuous GPS Observations (2000–2019). *Remote Sens*. 13(14):2725. https://doi.org/10.3390/rs13142725.

De Natale, G., Troise, C., Pingue, F., De Gori, P., & Chiarabba, C. (2001). Structure and dynamics of the Somma-Vesuvius volcanic complex. *Mineralogy and Petrology*, *73*, 5-22. https://doi.org/10.1007/s007100170007.

Del Pezzo, E., Chiodini, G., Caliro, S., Bianco, F., & Avino, R. (2013). New insights into Mt. Vesuvius hydrothermal system and its dynamic based on a critical review of seismic tomography and geochemical features. *Annals of Geophysics*. http://hdl.handle.net/2122/8832

Ducarme, B., Schueller, K. (2018): *Canonical Wave Grouping as the Key to Optimal Tidal Analysis. Bulletin d'Informations Marees Terrestres*, vol. 150, Bruxelles 2018.

Fores, B., Klein, G., Le Moigne, N., Francis, O. (2019). Long-term stability of tilt-controlled gPhoneX gravimeters. *Journal of Geophysical Research: Solid Earth*, 124, 12,264−12,276. https://doi.org/10.1029/2019JB018276.

Forster, F., Güntner, A., Jousset, P., Reich, M., Männel, B., Hinderer, J. & Erbas, K., (2021). Environmental and anthropogenic gravity contributions at the Þeistareykir geothermal field, North Iceland. *Geotherm Energy* 9, 26. https://doi.org/10.1186/s40517-021-00208-w.

Goodkind, J. M. (1999). The superconducting gravimeter, Review of Scientific Instruments, 70, 4131, doi:10.1063/1.1150092

Gottsmann, J., Rymer, H., & Berrino, G. (2006). Unrest at the Campi Flegrei caldera (Italy): A critical evaluation of source parameters from geodetic data inversion. *Journal of Volcanology and Geothermal Research*, *150* (1-3), 132-145.

Hector, B., Hinderer, J., Séguis, L., Boy, J.-P., Calvo, M., Descloitres, M., Rosat, S., Galle, S., Riccardi, U. (2014). Hydro-gravimetry in West-Africa: first results from the Djougou (Benin) superconducting gravimeter. *Journal of Geodynamics*, 80: 34-49. doi: 10.1016/j.jog.2014.04.003.

Hinderer, J., Crossley, D., & Warburton, R. (2015). *Superconducting gravimetry*. In T. Herring & G. Schubert (Eds.), Treatise on Geophysics, Geodesy (2nd ed., Vol. 3, pp. 66–122). Amsterdam: Elsevier.

Hinderer, J., Warburton, R.J., Rosat, S., Riccardi U., Boy J-P., Forster F., Jousset P., Güntner A., Erbas K., Little F., Bernard J.D. (2022). Intercomparing Superconducting Gravimeter Records in a Dense Meter-Scale Network at the J9 Gravimetric Observatory of Strasbourg, France. *Pure Appl. Geophys.* **179**, 1701–1727 (2022). https://doi.org/10.1007/s00024-022-03000-4.

Imbò, G., Bonasia V., Lo Bascio A. (1965). Variazioni della marea della crosta all'Osservatorio Vesuviano. *Ann. Osservatorio Vesuviano,* **7** (S6), 181-198.

Linde, N., Ricci, T., Baron, L., Shakas, A., & Berrino, G. (2017). The 3-D structure of the Somma-Vesuvius volcanic complex (Italy) inferred from new and historic gravimetric data. *Scientific reports*, 7(1), 1-10. DOI:10.1038/s41598-017-07496-y.

Manzella, A., Volpi, G., Zaja, A., & Meju, M. (2004). Combined TEM-MT investigation of shallow-depth resistivity structure of Mt Somma-Vesuvius. *Journal of Volcanology and Geothermal Research*, *131*(1-2), 19-32. https://doi.org/10.1016/S0377-0273(03)00313-5.

Meurers, B. (2002), Aspects of gravimeter calibration by time domain comparison of gravity records, Bulletin d'Information des Marées Terrestres, 135, 10643-10650.

Meurers B., Van Camp, M., & Petermans, T. (2007). Correcting superconducting gravity time-series using rainfall modelling at the Vienna and Membach stations and application to Earth tide analysis. *Journal of Geodesy*, 81(11), 703–712. https://doi.org/10.1007/s00190-007-0137-1.

Micro-g LaCoste, Inc. (2013). *gPhoneX Hardware Manual V3.1. http://microglacoste.com/wp-content/uploads/2017/06/gPhoneXmanual.pdf*. Accessed 4 Jan 2023.

Okubo S, Satomura M, Furuya M, Sun W, Matsumoto S, Ueki S, Watanabe H (2002) Grand design for the hybrid gravity network around the Mt. Fuji volcano. In: International Symposium on Geodesy in Kanazawa Abstract., pp 39–40.

Peterson, J. (1993). *Observations and modeling of seismic background noise* (Vol. 93, pp. 1-95). Reston, VA, USA: US Geological Survey.

Portier, N., Hinderer, J., Riccardi, U., Ferhat, G., Calvo, M., Abdelfettah, Y. & Bernard, J.-D. (2018). Hybrid gravimetry monitoring of Soultz-sous-Forêts and Rittershoffen geothermal sites (Alsace, France). *Geothermics*, 76, 201-219, https://doi.org/10.1186/s40517-018-0104-5.

Riccardi, U., Berrino, G., Corrado, G. (2002). Changes in instrumental sensitivity of some feedback systems used in LaCoste-Romberg gravimeters. *Metrologia*, 39, 509-515.

Riccardi, U., Berrino, G., Corrado, G., & Hinderer, J. (2008). Strategies in the processing and analyses of continuous gravity record in active volcanic areas: The case of Mt.Vesuvius. *Annals of Geophysics*, 51, 67–85.

Riccardi, U., Hinderer, J., Boy, J.-P., & Rogister, Y. (2009). Tilt effects on GWR superconducting gravimeters. *Journal of Geodynamics*, 48, 316–324. https://doi.org/10.1016/j.jog.2009.09.001.

Riccardi, U., Rosat, S., & Hinderer, J. (2011). Comparison of the Micro-g LaCoste gPhone-054 spring gravimeter and the GWRC026 superconducting gravimeter in Strasbourg (France) using a 300-day time series. *Metrologia*, 48, 28–39.

Riccardi, U., Rosat, S., Hinderer, J. (2012). On the Accuracy of the Calibration of Superconducting Gravimeters Using Absolute and Spring Sensors: a Critical Comparison, Pure and Applied Geophysics, 169, 1343-1356, https://doi.org/10.1007/s00024-011-0398-8.

Riccardi, U., Hinderer, J., Zahran, K., Issawy, E., Rosat, S., Littel, F., Ali, S.(2023). A First Reliable Gravity Tidal Model for Lake Nasser Region (Egypt). *Pure Appl. Geophys.* 180, 661–682. https://doi.org/10.1007/s00024-022-03087-9.

Rosat, S. & Hinderer, J. (2011). Noise levels of superconducting gravimeters: updated comparison and time stability. *Bull. Seism. Soc. Am*. 101(3).

Rosat, S. & Hinderer, J. (2018). Limits of detection of gravimetric signals on Earth. *Sci. Rep.*, 8, 15324. https://doi.org/10.1038/s41598-018-33717-z.

Rosat, S., Calvo, M., Hinderer, J., Riccardi, U., Arnoso, J. & W. Zürn (2015). Comparison of the performances of different Spring and Superconducting Gravimeters and a STS-2 Seismometer at the Gravimetric Observatory of Strasbourg, France, *Stud. Geophys. Geod*., 59, 58-82, https://doi.org/10.1007/s11200-014-0830-5.

Rosat, S., Hinderer, J., Crossley, D. & J.-P. Boy (2004). Performance of superconducting gravimeters from long-period seismology to tides, *Journal of Geodynamics*., 38, 3-5, 461-476, https://doi.org/10.1016/j.jog.2004.07.005.Rymer, H., & Brown, G. (1989). Gravity changes as a precursor to volcanic eruption at Poas volcano, Costa Rica. *Nature*, *342*(6252), 902-905.

Schüller, K. (2020). *Theoretical basis for earth tide analysis and prediction*. Manual-01-ET34-X-V, Surin, Thailand, PP. 217.

Scintrex Ltd. (2008) CG-5 Scintrex autograv system operation Manual, P/N 867700 Rev.4. Scintrex Limited, 2008. Concord, Ontario.

Sleeman R., van Wettum A. and Trampert J. (2006). Three-channel correlation analysis: a new technique to measure instrumental noise of digitizers and seismic sensors. Bull. Seismol. Soc. Amer., 96, 258-271.

Torge, W. (1989). *Gravimetry*. De Gruyter., Berlin–New York, PP. 465.

Van Camp, M., de Viron, O., Watlet, A., Meurers, B., Francis, O. & Caudron, C. (2017). Geophysics from terrestrial time-variable gravity measurements. *Reviews of Geophysics*, 55, 938–992. https://doi.org/10.1002/2017RG00056680.

van Ruymbeke, M. (1991). New Feedback Electronics for LaCoste and Romberg Gravimeters. Cah. Cent. Eur. Géodyn. Séismol., (4), 333–337.

Wahr, J. M., & Bergen, Z. (1986). The effects of mantle anelasticity on nutations, Earth tides, and tidal variations in rotation rate. Geophysical Journal of the Royal Astronomical Society, 64, 633–668.

Williams-Jones, G., & Rymer, H. (2002). Detecting volcanic eruption precursors: a new method using gravity and deformation measurements. *Journal of Volcanology and Geothermal Research*, *113*(3-4), 379-389.

Williams-Jones, G., Rymer, H., Mauri, G., Gottsmann, J., Poland, M., & Carbone, D. (2008). Toward continuous 4D microgravity monitoring of volcanoes. *Geophysics*, 73(6), WA19-WA28. https://doi.org/10.1190/1.2981185.

Wright, C.J., Hindley, N.P., Alexander, M.J., Barlow, M., Hoffmann, L., Mitchell, C. N., Prata, F., Bouillon, M., Carstens, J., Clerbaux, C., Osprey, S. M., Powell, N., Randall, C. E. and J. Yue (2022). Surface-to-space atmospheric waves from Hunga Tonga-Hunga Ha'apai eruption. Nature 609, 741-746. https://doi.org/10.1038/s41586-022-05012-5.

Zollo, A. E. A., Gasparini, P., Virieux, J., Le Meur, H., De Natale, G., Biella, G., ... & Vilardo, G. (1996). Seismic evidence for a low-velocity zone in the upper crust beneath Mount Vesuvius. *Science*, *274*(5287), 592-594. DOI: 10.1126/science.274.5287.592

	gPhone#116				iOSG#023				iGrav#029			
Wave	**Delta**	**RMS**	**Phase (°)**	**RMS (°)**	**Delta**	**RMS**	**Phase (°)**	**RMS (°)**	**Delta**	**RMS**	**Phase (°)**	**RMS (°)**
Q1	**1.141**	**0.0011**	**-0.459**	**0.057**	**1.14490**	**0.00019**	**-0.3001**	**0.0096**	**1.14455**	**0.00018**	**-0.2834**	**0.0092**
O1	**1.1475**	**0.00019**	**0.1466**	**0.0094**	**1.14795**	**0.00003**	**0.2042**	**0.0016**	**1.14769**	**0.00003**	**0.2121**	**0.0015**
NO1	1.1554	0.0031	0.67	0.15	1.15713	0.00052	0.4054	0.0257	1.15704	0.00050	0.412	0.025
K1	**1.13693**	**0.00013**	**0.1563**	**0.0068**	**1.13636**	**0.00002**	**0.3772**	**0.0012**	**1.13605**	**0.00002**	**0.3881**	**0.0011**
J1	1.1830	0.0030	-0.04	0.14	1.16265	0.00051	0.0635	0.0251	1.16261	0.00049	0.074	0.024
OO1	1.149	0.0033	0.58	0.16	1.16057	0.00056	0.2762	0.0275	1.15962	0.00053	0.280	0.026
NU1	1.220	0.019	1.31	0.90	1.2113	0.0033	0.2692	0.1552	1.2114	0.0032	0.07	0.15
2(KM)P1	0.98	0.123	-8.74	7.56	1.369	0.022	-5.6039	0.918	1.382	0.021	-5.62	0.87
3N2	1.30	0.068	18.31	2.99	1.2059	0.0088	4.4029	0.4157	1.1931	0.0089	4.26	0.43
2N2	1.168	0.0116	3.87	0.57	1.1683	0.0015	3.8742	0.0738	1.1665	0.0015	3.952	0.075
MUE2	1.1642	0.0079	2.80	0.39	1.1529	0.0010	3.1254	0.0505	1.1538	0.0010	3.208	0.051
N2	1.176	0.0014	3.623	0.069	1.17778	0.00018	3.3596	0.0088	1.17744	0.00018	3.3886	0.0089
NUE2	1.1898	0.0066	4.14	0.32	1.18248	0.00085	3.0124	0.041	1.18244	0.00086	3.091	0.042
M2	**1.18589**	**0.00013**	**2.412**	**0.0064**	**1.18612**	**0.00002**	**2.3884**	**0.0008**	**1.18584**	**0.00002**	**2.4081**	**0.0008**
L2	1.1828	0.0025	1.23	0.12	1.17715	0.00033	0.9494	0.016	1.17692	0.00033	0.963	0.016
S2	**1.19126**	**0.00025**	**1.144**	**0.012**	**1.18824**	**0.00003**	**0.9759**	**0.0015**	**1.18801**	**0.00003**	**0.997**	**0.0016**
ZETA2	1.72	0.084	-12.77	2.81	1.367	0.011	-11.8293	0.4526	1.369	0.011	-11.19	0.46
ETA2	1.28	0.025	-4.50	1.10	1.1898	0.0031	-2.6496	0.152	1.1896	0.0032	-2.60	0.15
2S2	1.52	0.12	29.12	4.71	1.533	0.016	-0.0313	0.5986	1.513	0.016	-0.97	0.61
2K2	0.807	0.064	1.97	4.57	1.2330	0.0083	7.6316	0.3853	1.2356	0.0084	7.39	0.39
2KN2	2.00	0.23	8.7	6.59	1.115	0.030	1.0805	1.5387	1.146	0.030	0.63	1.52
M2N3	0.76	0.42	103.01	31.99	1.274	0.039	11.0998	1.7496	1.205	0.045	9.97	2.15
MMUE3	0.97	0.36	61.7	21.2322	1.447	0.033	-0.4691	1.308	1.355	0.038	-1.68	1.62
MN3	1.083	0.069	-7.58	3.67	1.0864	0.0063	2.3488	0.3347	1.0829	0.0074	1.82	0.39
MNUE3	1.57	0.33	-37.0	12.18	1.307	0.031	4.3999	1.3408	1.252	0.035	3.28	1.62
M3	1.0878	0.0095	-0.86	0.50	1.0639	0.00088	0.957	0.0472	1.0644	0.0010	0.869	0.055
RMSE	17.3 nm/s^2				3.62 nm/s^2				3.54 nm/s^2			
Pres. Admit.	-2.79 ± 0.030 nm/s^2/hPa				-2.78 ± 0.018 nm/s^2/hPa				-2.80 ± 0.017 nm/s^2/hPa			

Table S1: Results (Delta factor and Phase) and RMS errors of the unfiltered tidal analyses obtained with ET34-X-V80 software (Schuller, 2020) for the gPh#116 gravimeter and two Superconducting gravimeters collocated at J9 gravity Observatory (Strasbourg-France); Air-Pressure admittance and root mean square error (RMSE) of the observations are listed too. The results are used for the relative calibration of the gPh#116; the largest tidal waves are highlighted in bold.

Wave	Delta	RMS	Phase (°)	Std (°)
Mm	1.176	0.024	2.01	1.21
Mf	0.945	0.014	-6.42	0.86
Q1	1.1463	0.00064	0.324	0.032
O1	1.1478	0.00013	0.3421	0.0065
NO1	1.152	0.0019	1.016	0.095
P1	1.1475	0.00034	0.087	0.017
S1K1	1.1353	0.00010	0.233	0.0047
J1	1.160	0.0017	-0.437	0.084
OO1	1.143	0.0025	0.63	0.12
NU1	1.047	0.012	-0.42	0.67
2(KM)P1	1.205	0.058	-8.73	2.76
3N2	1.226	0.027	19.24	1.26
2N2	1.155	0.0032	2.62	0.16
MUE2	1.161	0.0026	1.8108	0.13
N2	1.17886	0.00043	1.32	0.02
NUE2	1.15935	0.0021	1.36	0.11
M2	1.17821	0.00007	0.8471	0.0036
L2	1.168	0.0013	0.540	0.066
S2	1.1746	0.00015	0.2163	0.0074
K2	1.1700	0.00047	0.508	0.0023
ZETA2	0.977	0.037	7.80	2.19
ETA2	1.158	0.0096	-1.07	0.47
2S2	1.12	0.049	-0.88	2.51
2K2	1.35	0.026	7.69	1.08
2KN2	0.58	0.12	-14.78	11.86
M2N3	1.58	0.076	-2.77	2.74
MMUE3	1.64	0.077	9.49	2.69
MN3	1.099	0.014	0.87	0.71
MNUE3	1.39	0.072	3.44	2.98
M3	1.062	0.0034	1.04	0.18
RMSE: 16.73 nm/s^2				
Air-Pressure admittance: -3.74 ± 0.010 $nm/s^2/hPa$				

Table S2: Results (Delta factor and Phase) and RMS errors of the unfiltered tidal analyses obtained with ET34-X-V80 software (Schuller, 2020) on 174 days of gravity recording collected with the gPh#116 gravimeter at Mt. Somma-Vesuvius permanent station; Air-Pressure admittance and root mean square error (RMSE) of the observations are listed too.